A&A 382, 256–281 (2002)
DOI: 10.1051/0004-6361:20011580

Astronomy & Astrophysics

Mineral formation in stellar winds

III. Dust formation in S stars

A. S. Ferrarotti and H.-P. Gail

Institut für Theoretische Astrophysik, Universität Heidelberg, Tiergartenstraße 15, 69121 Heidelberg, Germany

Received 20 June 2001 / Accepted 5 November 2001

Abstract. S stars are transition objects at the top of the AGB between M-and C-stars. The third dredge-up in thermally pulsating AGB-stars transports freshly synthesised carbon from the He burning zone into the stellar atmosphere. If the carbon and oxygen abundance are about equal the star is classified as being of spectral type S. Stars at the top of the AGB are subject to large mass-loss caused by a strong stellar wind. At some distance from the star the temperature of the gas drops below the condensation temperature of some mineral compounds and soot. This results in optically thick dust shells which are sources of an intense IR-radiation from warm dust. The composition of the dust formed in the stellar outflow critically depends on the C/O-ratio. For the standard element mixture characteristic for main sequence stars one has C/O < 1 (M-stars) and the O not bound in CO forms a mineral assemblage which is dominated by Mg-Fe-silicates and metallic Fe. For C/O > 1 (C-stars) the dust mixture is dominated by solid carbon and some SiC. The element mixture of S stars is characterised by the non-availability of sufficient quantities of O or C to form the standard condensates. We have investigated the condensation processes for the peculiar element mixture at the M-S-C transition on the AGB. From thermodynamic equilibrium calculations we find that the most likely solids to be formed are solid FeSi, metallic iron and small quantities of forsterite and SiC. Nucleation of dust may be triggered by TiC, ZrC or TiO_2. For these substances, non-equilibrium dust condensation in the outflow is calculated for a simple stationary wind model for a sample of C/O-ratios. The results of our calculation show that iron and FeSi dust condensates in the circumstellar shells of S stars.

Key words. circumstellar matter – dust – stars: mass-loss – stars: winds – stars: AGB and post-AGB

1. Introduction

All medium mass stars with inital main sequence masses $2 \lesssim M_* \lesssim 8\ M_\odot$ evolve at the end of their life towards the asymptotic giant branch (AGB) where they become cool luminous giant stars (e.g. Iben 1991). At this stage of their evolution they enter the region of massive mass-loss in the HR-diagram (cf. Fig. 5 of de Jager et al. 1988) where cool stars with heavy mass-loss develop a dense circumstellar dust shell which is easely detected by its infrared emission from hot dust.

This dust is a mixture of different fine grained minerals which condense in the cooling outflow from the gas phase. The composition of the condensates critically depends on the element composition of the stellar surface, as can be seen, for instance, from the condensation sequences calculated by Lattimer et al. (1978). Corresponding to the three completely different spectral appearances of cool stars on which their classification as being of spectral type M, S, or C is based on, three substantially different chemical compositions of the stellar surfaces are observed. The basic property responsible for the differences in the spectra of M, S, or C stars is the abundance ratio of oxygen to carbon, as has been recognised by Fujita (cf. Warner 1968). M stars are characterised by an excess of oxygen over carbon which enables the formation of oxygen bearing compounds like TiO molecules in the stellar atmosphere and the condensation of Mg-Fe-silicates, Ca-Al-compounds, and other minerals in the outflow (e.g. Grossman 1972). C stars are characterised by an excess of carbon over oxygen which enables the formation of C_2, CN and other carbon bearing molecular compounds in the stellar atmosphere and the condensation of soot, carbides, sulfides and nitrides in the outflow (e.g. Lattimer et al. 1978). S stars have approximately equal abundances of oxygen and carbon and are different in their chemical properties from both their oxygen and carbon rich relatives.

Send offprint requests to: H.-P. Gail,
e-mail: gail@ita.uni-heidelberg.de

In this paper we study the dust formation process in S stars when during stellar evolution upwards on the AGB the carbon abundance increases stepwise by third "dredge up" episodes and the star passes through the stage of an S star. From chemical equilibrium calculations we determine the possible condensates for a range of carbon to oxygen ratios at the transition from oxygen- to carbon rich element mixtures and determine which materials may be formed as major and minor dust species, and which condensates may act as seed particles for the more abundant dust species.

This information is used to calculate the condensation of a multi-component dust mixture in a stellar outflow by solving the corresponding set of kinetic equations for dust formation simultaneously with the equations for a stellar wind. As model for a stellar outflow we choose the rather simplistic model of a stationary wind since time dependent wind models considering the pulsation of the underlying star presently cannot be combined with modelling of the formation of multicomponent dust mixtures.

This paper extends the previous studies on dust formation in M stars (Gail & Sedlmayer 1999, henceforth called Paper I) and on the compositional dependence of the mineral mixture in M stars on the Mg/Si abundance ratio (Ferrarotti & Gail 2001, henceforth called Paper II), to AGB stars in the transition state between M and C stars.

The plan of this paper is as follows: in Sect. 2 we review briefly some properties of S stars, in Sect. 3 we discuss the chemical composition of the gas phase at the M-S-C transition, in Sect. 4 we discuss the variation of the chemical equilibrium composition of simple gas-solid mixtures with varying carbon to oxygen abundance ratios at the M-S-C transition, in Sect. 5 we give some comments on the nucleation process, and in Sect. 6 we discuss the set of equations for calculating dust formation under non-equilibrium conditions. Section 7 presents the results of model calculations for dust formation in stationary outflows and Sect. 8 gives some concluding remarks.

2. Physical properties of S stars

In this paper we consider the formation of dust in the circumstellar shells of *intrinsic* S-stars, which are presently in the "third dredge-up" phase on the AGB.

2.1. Stellar evolution and the M-S-C transition

Stars with initial masses in the range $2 \lesssim M_* \lesssim 8\,M_\odot$ on the main sequence finally arrive on the AGB where they become efficient dust factories. Initially their element mixture is close to the standard element mixture which they inherited from their parent molecular cloud at time and position of their birth within the galaxy. Some minor changes occur during the first and second "dredge-up" episodes on the RGB and early AGB during which the abundance of He slightly and that of N considerably increases while the C abundance slightly decreases (e.g. Boothroyd & Sackman 1999). These abundance changes do not significantly affect abundances of those elements which are of potential interest for dust condensation.

As the stars enter the thermally pulsing upper part of the AGB, after a few pulses the surface abundances of some elements start to change by the third "dredge-up" episode due to mixing of products of H and He burning into the convective envelope. The most important event is the stepwise increase of the carbon abundance, following each thermal pulse in the core region, from a C/O abundance ratio of about 0.4 to C/O > 1, after which the star becomes a carbon star (e.g. Groenewegen et al. 1995; Lattanzio & Forestini 1999; Busso et al. 1999). If the C/O abundance ratio is close to unity, the star appears as of spectral type S (Scalo & Ross 1976). For low initial masses of the star ($M_* \lesssim 2\ M_\odot$), the C/O ratio increases in a few and rather big steps from C/O < 1 to C/O > 1 and the intermediate state of C/O ≈ 1 of an S star probably is skipped in most cases (Groenewegen et al. 1995). Stars with higher initial masses experience a bigger number of thermal pulses with smaller individual increases of the C/O abundance ratio following each pulse. These stars are likely to become S stars for a certain period of time until they develop into C stars.

The third "dredge-up" also changes the abundances of some other elements. The abundance of He and N somewhat increases, but this has no consequences for the dust formation problem. At the same time the abundances of *s*-process elements beyond the iron peak strongly increase by factors of $10 \ldots 100$, but generally the abundances of such elements are too low for being of importance for the dust formation problem, except perhaps for Mo and Zr, which may be important for the formation of seed nuclei for dust growth (Bernatowicz et al. 1996). The abundances of the less heavier elements from Mg to Fe are not significantly affected by burning processes during the AGB stage, only some less abundant isotopes show significant abundance changes. The most important refractory elements from Mg to Fe essentially retain their main sequence abundances.

Intermediate mass stars with initial masses between $4 \ldots 5\ M_\odot$ and $8\ M_\odot$ most likely experience hot "bottom burning". These stars do not become carbon stars (cf. Lattanzio & Forestini 1999) and probably they also do not become real S stars. They develop a strong N overabundance which, however, is of no importance for the dust formation problem.

2.2. Element abundances

The special element abundances characteristic for S-stars, thus, develop during the evolution of stars with initial masses between about $2\,M_\odot$ and about $4\,M_\odot$. The rather short life time of such stars of at most $\approx 2\times 10^9$ years means that galactic stars presently observed to be in the S star stage of their evolution have pop I metallicities. Estimated average abundances of some elements for pop I metallicity at the time of onset of significant dust production are

Table 1. Elemental abundances for the solar system (Anders & Grevesse 1989; Grevesse & Noels 1993) and adopted abundances for stars on the asymptotic giant branch.

El.	$\epsilon_{\rm solar\ system}$	$\epsilon_{\rm AGB}$		
	M	M	S	C
He	9.75×10^{-2}	1.04×10^{-1}	1.04×10^{-1}	1.04×10^{-1}
C	3.55×10^{-4}	2.33×10^{-4}	6.87×10^{-4}	8.24×10^{-4}
N	9.33×10^{-5}	2.52×10^{-4}	2.52×10^{-4}	2.52×10^{-4}
O	7.41×10^{-4}	6.87×10^{-4}	6.87×10^{-4}	6.87×10^{-4}
Mg	3.85×10^{-5}	3.85×10^{-5}	3.85×10^{-5}	3.85×10^{-5}
Si	3.58×10^{-5}	3.58×10^{-5}	3.58×10^{-5}	3.58×10^{-5}
S	1.85×10^{-5}	1.85×10^{-5}	1.85×10^{-5}	1.85×10^{-5}
Ti	8.60×10^{-8}	8.60×10^{-8}	8.60×10^{-8}	8.60×10^{-8}
Fe	3.24×10^{-5}	3.24×10^{-5}	3.24×10^{-5}	3.24×10^{-5}
Zr	4.09×10^{-10}	4.09×10^{-10}	4.09×10^{-9}	8.00×10^{-9}

shown in Table 1 in the second column. Columns 3 and 4 show estimated abundances for S and C stars, respectively. Column 1 shows "solar system" abundances for comparison.

These abundances on the early AGB are estimated as follows: For He, C, N, and O we scaled the standard cosmic abundances as given by Anders & Grevesse (1989) and Grevesse & Noels (1993) according to the change in stellar surface abundances found in the evolutionary calculations of Schaller et al. (1992) for stars of small and intermediate masses. The results agree with observationally determined mean abundances in AGB stars (Smith & Lambert 1990). For the more heavier elements from Na up to the iron peak burning temperatures in intermediate mass AGB stars are too low in order to change the abundance of the major isotopes of such elements. We can use for these elements their main sequence abundances.

The abundances of Mg and Si given in Table 1 for M, S, and C stars are those given by Anders & Grevesse (1989) for the solar system. They are not really representative for average cosmic abundances, where the Mg/Si abundance ratio is somewhat higher (cf. Edwardsson et al. 1993; Snow & Witt 1996). The dependence of the composition of the mineral mixture formed in circumstellar shells on the Mg/Si ratio is discussed in Ferrarotti & Gail (2001). In order to keep the number of parameters in our present discussion low, we restrict all calculations to Solar System abundances for the elements from Mg to Fe (cf. Table 1).

The chemistry to be considered for dust formation during the AGB stage of evolution of intermediate mass stars at the M-S-C transition essentially reduces to the problem of studying the condensation problem for an element mixture of the type defined by the second mixture in Table 1, but with increasing C abundance up to C/O ratios slightly exceeding unity, keeping fixed the abundances of all the other elements.

2.3. Oberved dust properties

Circumstellar dust shells are observed to exist for intrinsic S stars only. Extrinsic S stars show no indications for the presence of a circumstellar dust shell (Jorissen et al. 1993), in accord with the current understanding that only intrinsic S stars are on the AGB.

For S stars Chen & Kwok (1993) have collected IRAS LRS spectra, which show that these stars either show a featureless dust continuum or weak silicate emission features. A few stars show a weak SiC emission feature. The objects in their list showing strong silicate emission have been shown by Lloyd Evans & Little-Marenin (1999) to be misclassified M stars in nearly all cases. The stars with medium and weak silicate emission (group E in Chen & Kwok 1993) and with a featureless continuum (group F) in those cases, where the presence or absence of Tc is known, generally show Tc and, thus, are AGB stars. From the relatively large number of objects in Chen & Kwok (1993) with seemingly pure stellar continuum emission without detectable dust emission (their group S) a considerable fraction, but not all of them, are extrinsic S stars.

Thus, the main characteristic of the infrared emission from circumstellar dust around S stars, if detectable, is a featureless continuum emission with partially superposed weak emission bands from silicate dust or, in a few cases, from SiC dust. This featureless continuum resembles much the dust emission properties of C stars, as has been noted by Jura (1988).

2.4. Mass-loss rates and outflow velocities

Mass-loss rates of S stars have been derived from observed microwave lines of CO by Jorissen & Knapp (1998) and Groenewegen & de Jong (1998). For intrinsic S stars, observed mass-loss rates range from 10^{-7} to $10^{-5}\ M_\odot\,{\rm yr}^{-1}$. Terminal velocities of stellar winds also are determined from observations of CO lines. Groenewegen & de Jong (1998) and Jorissen & Knapp (1998) present compilations of known data and some new determinations. Observed outflow velocities of intrinsic S stars are almost evenly distributed in the range from 5 to 20 $\rm km\,s^{-1}$.

2.5. Stellar parameters

Kerschbaum (1999) and Kerschbaum & Hron (1996) have modeled with some success the global shape of the spectral energy distribution of stars with circumstellar dust shells with two black-body energy distributions, one for the central star and a second one for the shell. The derived equivalent black body temperatures of the stars is for S stars of the order of 2500 K. This is consistent with results for temperatures determined by van Belle et al. (1997). In our model calculations we approximate the stellar radiation field by a 2500 K black body.

Stellar luminosities for galactic S stars based on Hipparcos parallaxes have been derived for a number of stars by Van Eck et al. (1998). They find that for most

stars $5 \times 10^3 \lesssim L_* \lesssim 1 \times 10^4\ L_\odot$. This agrees with the findings of van Belle et al. (1997) and with the HR-diagram position of Magellanic cloud S stars (Lloyd Evans 1984). In our model calculations we use the canonical value of $L_* = 10^4\ L_\odot$ generally used in theoretical model calculations for circumstellar dust shells. This is within the observed range for real stars, thought at its upper limit. Lower luminisities would result in somewhat lower degrees of condensation and lower expansion velocities.

3. Chemical equilibrium composition of the gas phase

Dust in a circumstellar outflow is formed from the atomic and molecular species of the gas phase. The chemical composition of the gas determines the kind of particles which are available for the dust formation process and the chemical reactions which are possible for dust formation. Any discussion of dust formation naturally has to begin with the chemistry of the gas phase. This is already one of the basic difficulties one encounters in this context: the structure of the outer layers of late tape giants is rather complex because these stars are located in a region of the Hertzsprung–Russel diagram where the AGB crosses the instability strip (e.g. Wood 1990a, 1990b; Gautschy & Saio 1995; Xiong et al. 1998). The stellar photosphere and the adjacent outflow region therefore are regularly traversed by running shock waves (cf. Willson 2000) excited by the stellar pulsation which dissociate molecules and ionise atoms by the sudden temperature rise behind the shock. Subsequent cooling leads to recombination to neutral atoms and re-formation of molecules. This makes the determination of the chemical composition in the region between the stellar photosphere and the dust forming layer several stellar radii outside of the star an extremely difficult task, which has not adequately be solved up to now. Not to mention additional problems resulting from the possible existence of chromospheres in part of these stars which may be sources of an UV emission which possibly drives a strong non-equilibrium chemistry (Beck et al. 1992).

There have been some attempts to model the chemistry in the stellar outflow by means of reaction kinetics (cf. Glassgold 1996, and references therein), but due to the vast uncertainties of such models it is by no means sure that presently such calculations yield results which are more realistic than chemical equilibrium calculations. For this reason one often takes recourse chemical equilibrium calculations assuming that the true composition of the gas, at least with respect to the abundant molecules, is not very different from a chemical equilibrium composition. This hypothesis is based on the observation, that at elevated temperatures above $T \gtrsim 1000\,\mathrm{K}$ only very simple molecules (containing at most a few atoms) with a particular high bond energy are formed in chemical equilibrium. These molecules should in any case be the most abundant ones, even in a non-equilibrium state. The only difference would be that the relative abundances of such molecules predicted by chemical equilibrium would be slightly in error. The abundances of minor components, however, could be very different in non-equilibrium as compared to equilibrium calculations and if some important reaction involved in the dust formation process depends on such minor species this would invalidate the equilibrium assumption.

Table 2. Molecules considered in the chemical equilibrium calculation.

Element	Molecules
H	H, H_2
C	C, CH_4, C_2, C_2H, C_2H_2
O	O, OH, H_2O, CO, CO_2
N	N, N_2, CN, HCN, NH_3, AlN
Si	Si, SiO, SiC, SiC_2, Si_2C, Si_2C_2, SiS, SiH
S	S, CS, HS, H_2S, AlS, FeS, CaS
Al	Al, AlO, AlOH, Al_2O, AlH, AlCl
Mg	Mg, MgO, MgH, MgS
Fe	Fe, FeO, $Fe(OH)_2$, FeH, AlFe,FeSi
Ca	Ca, CaOH, $Ca(OH)_2$, CaF, CaF_2
Na	Na, NaH, NaCl
Cr	Cr, CrH, CrO, CrO_2, CrO_3
Mn	Mn, MnO, MnH, MnS
K	K, KO, KH, KOH
Ti	Ti, TiO, TiO_2, TiC_2, TiC_4, TiS
V	V, VO, VO_2
Zr	Zr, ZrO, ZrC_2, ZrC_4, ZrCl, ZrS, ZrN
Cl	Cl, HCl, CaCl, $CaCl_2$, TiCl, TiOCl
F	F, HF, TiF, TiF_2, AlOF

If the chemistry in the outflow is dominated by ion-molecule reactions, the chemistry would be completely different from equilibrium chemistry, but it seems unlikely that ion-molecule chemistry is dominating in the warm and rather dense region between the star and the dust forming layer.

In the following we neglect all the problems resulting from a possible non-equilibrium chemistry of the gas phase and calculate the chemical equilibrium composition of a solid-gas mixture at the M-S-C transition. The purpose is to determine the most abundant molecules in the gas phase available for the condensation process and the most stable solid compounds which are the likely candidates for condensation in the stellar wind. The results then will be used as input information in our non-equilibrium model calculation of dust condensation in the cooling flow.

3.1. Calculation of chemical equilibria

The chemical composition of the solid gas mixture in a circumstellar shell is calculated from two sets of equations: (i) the set of laws of mass action for the individual compounds, and (ii) the constraints set by the element

abundances. The principles of this calculation are described in Paper II.

Polynomial approximations for calculating the required changes of free enthalpy ΔG for the formation of the molecules and solids from free atoms are taken from Sharp & Huebner (1990). For some molecules and solids not contained in that list polynomial approximations of the type used by Sharp & Huebner have been calculated from data taken from the JANAF tables (Chase et al. 1985) or Barin (1992). An error in the JANAF data for HS detected by Ebel & Grossman (2000) has been corrected. Results for some Fe-Si-compounds are given in appendix B. The set of molecules considered in our calculation of the gas-phase composition is listed in Table 2.

3.2. Molecular composition of the gas phase

First we determine the composition of the gas phase at the M-S-C transition in order to determine the abundant molecular species which can be responsible for the formation and growth of dust under non-equilibrium conditions. This calculation considers the 19 most abundant elements and their approximately 100 most stable molecular compounds. Solids are not included for the moment. The molecular composition of a gas with this element mixture is calculated for a pressure of $P = 10^{-4}$ dyn cm^{-2} and for the temperature region between $600 \leq T \leq 1600$ K. This pressure P and this temperature interval T are representative for the conditions under which condensation can be expected to occur in the wind of Red Giant stars.

Figure 1 shows the variation of molecular abundances for some important molecules with increasing carbon/oxygen abundance ratio in the transition region between M and C stars for $T = 1000,\ 1200$ and 1600 K and a pressure of $P = 10^{-4}$ dyn cm^{-2}. The figure shows that at low temperatures (top and middle picture) there occurs a dramatic change in the gas phase composition at a critical carbon abundance of

$$\epsilon_{\rm C,crit} = \epsilon_{\rm O} - \epsilon_{\rm Si} + \epsilon_{\rm S}\,. \tag{1}$$

For the element abundances given in Table 1 this corresponds to

$$\frac{\epsilon_{\rm C,crit}}{\epsilon_{\rm O}} = 0.975\,. \tag{2}$$

At this particular carbon/oxygen abundance ratio, the elements C, O, Si, and S are completely bound in the three molecules CO, SiO, and SiS. No other compounds of these elements exist with significant abundance for a carbon abundance close to $\epsilon_{\rm C} = \epsilon_{\rm C,crit}$. The complete mutual fixing of C, O, Si, and S at this special value of $\epsilon_{\rm C}$ results from the extraordinary high bond energies of the three molecules (CO: 1076.5, SiO: 799.6, SiS: 623 kJ mol^{-1}). Only the N_2 molecule (not shown in the figure) has a comparably high bond energy (945.3 kJ mol^{-1}), which results in (nearly complete) complete fixing of nitrogen in this molecule.

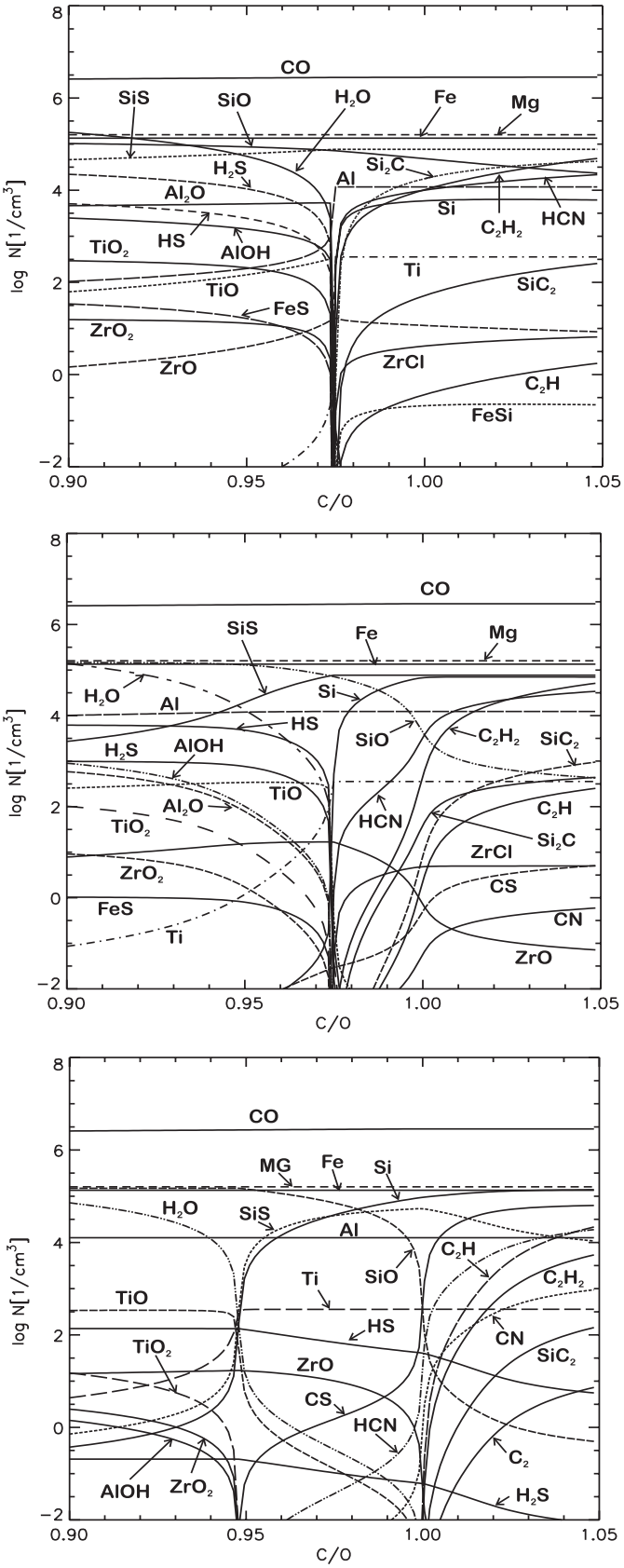

Fig. 1. Variation of some molecular abundances of interest for the dust formation problem with increasing C/O–ratio for conditions typical for the condensation zone in circumstellar dust shells: $T = 1000$ K (top), $T = 1200$ K (middle), and $T = 1600$ K (bottom), $P = 10^{-4}$ dyn cm^{-2}.

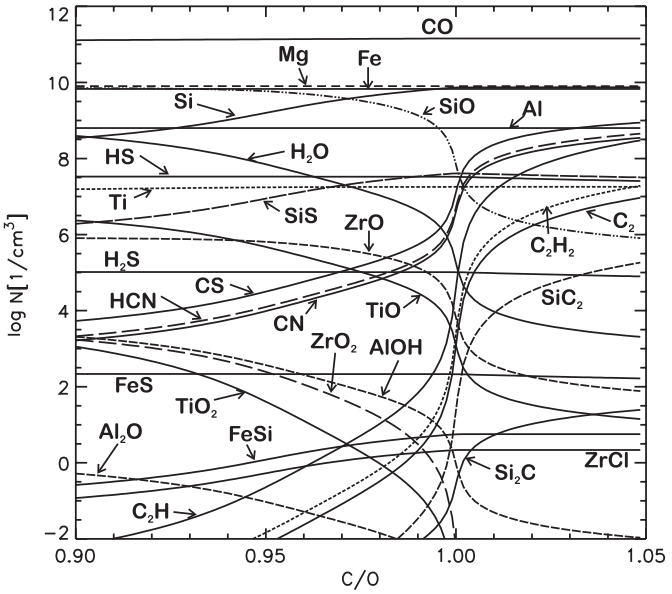

Fig. 2. Variation of some molecular abundances with varying C/O abundance ratio for the stellar photosphere: $T = 2500\,\mathrm{K}$, $P = 10^2\,\mathrm{dyn\,cm^{-2}}$).

If the carbon abundance is less than the critical abundance $\epsilon_{\mathrm{C,crit}}$ then part of the oxygen is available for forming oxygen bearing molecules while in the opposite case some carbon is left over which forms carbon bearing molecules. Hence, with increasing $|\epsilon_{\mathrm{C}} - \epsilon_{\mathrm{C,crit}}|$ the molecular composition approaches the standard compositions of M or C stars.

For temperatures around $\approx$1600 K this change of the molecular composition of the gas phase in the transition region between M and C stars does not occur at $\epsilon_{\mathrm{C}} = \epsilon_{\mathrm{C,crit}}$ but at the somewhat lower carbon abundance of $\epsilon_{\mathrm{C}} = \epsilon_{\mathrm{O}} - \epsilon_{\mathrm{Si}}$ (=$0.948\epsilon_{\mathrm{O}}$ for the element abundances given in Table 1), as can be seen in the bottom picture of Fig. 1. The reason for this is the slightly lower bond energy of SiS as compared to CO and SiO. The SiS molecule disappears above $T \approx 1600\,\mathrm{K}$ and then all the Si is bound in SiO up to the temperature where SiO disappears.

Within the stellar photosphere the temperature and pressure are much higher than in the dust shell. The variation of abundance of some important molecules with varying carbon to oxygen ratio for this case is shown for comparison in Fig. 2 for $T = 2500\,\mathrm{K}$ and $P = 10^2\,\mathrm{dyn\,cm^{-2}}$. This closely corresponds to the results shown by Scalo (1974). The transition between the oxygen dominated and carbon dominated chemistry occurs at $\epsilon_{\mathrm{C}} \approx \epsilon_{\mathrm{O}} - \epsilon_{\mathrm{Si}}$. The change in the chemical composition is much softer in the stellar atmosphere than in the circumstellar condensation zone and extends to a higher carbon to oxygen ratio than in the dust forming layer.

In particular with increasing C/O ratio the last oxygen bearing molecules disappear and the first carbon bearing molecules appear in the stellar atmosphere within a narrow interval $(0.99 \ldots 1.01)$ of the C/O abundance ratio around $\epsilon_{\mathrm{C}} = \epsilon_{\mathrm{O}}$. This holds especially for the diagnostically important ZrO, C_2, and CN molecules (Scalo & Ross 1976). This is the region of C/O ratios where stars would be classified as being of spectral type SC. In the interval of C/O abundances from $\approx$0.95 to $\approx$0.99 the star would be classified as being of spectral type S because of the dominance of ZrO over TiO (Scalo & Ross 1976). For the S stars, there obviously exists a region of C/O ratios $\epsilon_{\mathrm{C,crit}} \lesssim \epsilon_{\mathrm{C}} \lesssim \epsilon_{\mathrm{O}}$ where the atmospheric composition of the star is only moderately depleted from O bearing molecules and carbon bearing molecules are absent, while the chemistry in the dust forming layer (if equilibrium chemistry can be applied to this region) is definitely of carbon-rich nature as for stars with the spectral characteristics of carbon stars.

4. Chemical equilibrium condensation

We start our discussion of dust condensation in the outflow from S stars with a discussion of chemical equilibrium condensation for the mixture of elements defined in Table 1. This mixture is different from the carbon or oxygen rich element mixtures for which solid-gas phase equilibria have been discussed so far in astrophysical contexts: Grossman (1972), Lattimer et al. (1978), Saxena & Ericksson (1986), Sharp & Huebner (1990), Lodders & Fegley (1995), Sharp & Wasserburg (1995), just to mention a few of the many papers on this subject. For an extended (though not complete) list of references to equilibrium studies see Lodders & Fegley (1997, 1999). The dust formation process in stellar winds is a process which clearly operates under conditions which are quite far from thermal equilibrium conditions. One cannot expect that exactly the mixture of solids predicted by equilibrium chemistry condenses in such an environment. Also, true condensation temperatures in the outflow may be quite different from condensation temperatures in chemical equilibrium. Nevertheless it is very instructive to determine the possible condensates and their stability limits from such considerations since this helps to single out from the vast number of possibilities the few solid compounds which are the most likely ones to condense because of their stability up to very high temperatures in the given environment.

Equilibrium calculations and observation show that silicate compounds form the most abundant dust components in the shells of oxygen rich stars and carbon compounds the most abundant compounds in carbon rich stars. Some impression how the nature of the condensates changes at the transition from M to C stars may be obtained from Gilman (1969) and Lodders & Fegley (1995). We consider now in some detail the stability limits and equilibrium abundances of the important dust species in the transition regime between M and C stars where the carbon to oxygen abundance ratio changes from C/O < 1 to C/O > 1.

In the calculations described below we examine the possible condensation of 90 solids for a state with constant pressure $P = 10^{-4}\,\mathrm{dyn\,cm^{-2}}$ in the temperature

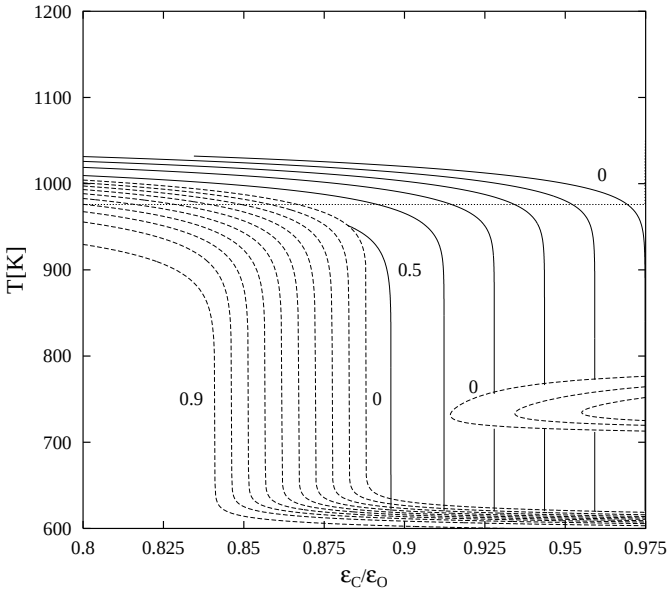

Fig. 3. Equilibrium condensation of forsterite (full line) and enstatite (dashed line) at $P = 10^{-4}\,\mathrm{dyn\,cm^{-2}}$ for varying C/O–ratios. The numbers at the lines denote the degree of condensation f of Si in the solids. Below the stability limit of enstatite both enstatite and forsterite coexist in chemical equilibrium. For clarity only the equi-abundance lines of enstatite are shown in the region of coexistence of forsterite and enstatite. The dotted line shows the condensation limit of solid iron.

region between $600 \le T \le 1600$ K. They are selected from the JANAF tables (Chase et al. 1985), Barin (1992), and Kubaschewski & Alcock (1983), according to high abundances of the elements from which they are formed and a high vapourisation or sublimation temperature. The molecules considered in the calculation are listed in Table 2.

4.1. Condensation of silicates in the regime $\epsilon_C < \epsilon_{C,crit}$

In an oxygen rich environment, corresponding to carbon abundances less than the critical carbon abundance $\epsilon_{\mathrm{C,crit}}$ defined by (1), olivine with composition $Mg_{2x}Fe_{2(1-x)}SiO_4$ $(0 \le x \le 1)$, pyroxene with composition $Mg_xFe_{1-x}SiO_3$ $(0 < x \le 1)$ and metallic iron are the most stable compounds involving only the most abundant refractory elements. Radiation from warm dust of this kind dominates the infrared emission from the dust shells around M stars. Calculation of the composition of heterogeneous equilibria show that they remain the most stable compounds formed from the abundant elements C, N, O, Mg, Si, S, Fe up to the limit $\epsilon_{\mathrm{C,crit}}$, but with some important changes with respect to the degree of condensation. We consider now the details in the transition region.

In chemical equilibrium the silicates are nearly iron free (cf. Saxena & Ericksson 1986), except at low temperatures $T \lesssim 500\,\mathrm{K}$ where chemical equilibrium does not hold in a circumstellar shell. For simplicity we have considered in our calculations only the iron free compounds forsterite (Mg_2SiO_4) and enstatite ($MgSiO_3$). In M stars, forsterite condenses at a slightly higher temperature than enstatite (cf. Gail & Sedlmayr 1999). This remains true also in the transition region up to the critical carbon abundance $\epsilon_{\mathrm{C,crit}}$ if ϵ_{C} approaches ϵ_{O} from below. Figure 3 shows the result of an equilibrium calculation for the equilibrium between forsterite, enstatite and the gas phase, but without considering any other solid. In particular Fig. 3 shows the dependence of the degree of condensation of forsterite and enstatite on the carbon to oxygen abundance ratio in the transition region relevant for S stars. In the region of coexistence of forsterite and enstatite, only the equi-abundance lines of enstatite are shown for clarity. The behaviour of the equi-abundance lines of forsterite in that region is complex and is not needed for our further discussion.

Up to a carbon abundance of

$$\epsilon_{\mathrm{C}} = \epsilon_{\mathrm{O}} - 3\epsilon_{\mathrm{Si}} \tag{3}$$

($\epsilon_{\mathrm{C}}/\epsilon_{\mathrm{O}} = 0.844$ for the element mixture defined in Table 1) one finds the usual picture: olivine condenses first and its degree of condensation rapidly increases with decreasing temperature until the available magnesium is nearly completely bound in forsterite. This consumes only one half of the available Si because of $\epsilon_{\mathrm{Si}} \approx \epsilon_{\mathrm{Mg}}$. For lower temperatures the forsterite converts into enstatite until the Si is completely bound in enstatite and some forsterite. Up to a carbon abundance defined by (3) the silicate dust can be formed as in standard M stars. This corresponds to stars which would be classified according to their spectra as normal M stars or at most as mild MS stars (Scalo & Ross 1976).

For carbon abundances exceeding the limit (3) the available O (i.e. the excess of O over C) does not suffice to fix the fraction of the Si, which cannot be bound in forsterite, in the less stable mineral enstatite. With increasing carbon to oxygen abundance ratio a decreasing fraction of the Si condenses into enstatite. At a carbon abundance above

$$\epsilon_{\mathrm{C}} = \epsilon_{\mathrm{O}} - 2\epsilon_{\mathrm{Mg}} \tag{4}$$

($\epsilon_{\mathrm{C}}/\epsilon_{\mathrm{O}} = 0.888$ for the element mixture defined in Table 1) the available oxygen is reduced to such an extent that the formation of forsterite is no more limited by the magnesium abundance. Then, no enstatite but only the most stable silicate mineral forsterite is formed in the abundance interval between the lower limit given by (4) and the upper limit $\epsilon_{\mathrm{C,crit}}$, except for the small island of stability of $MgSiO_3$ shown in Fig. 3. The excess magnesium which is not consumed by silicate formation then forms a different solid compound which turns out to be MgS.

The oxygen bound in CO usually is not available for the formation of silicates because of its high bond energy. Only at rather low temperatures net reactions of the type

$$\mathrm{Si} + 2\mathrm{Mg} + 4\mathrm{CO} + 2\mathrm{H_2} \longrightarrow \mathrm{Mg_2SiO_4(solid)} + 2\mathrm{C_2H_2}$$

become thermodynamically favourable. This is responsible for the condensation of Si into forsterite and enstatite

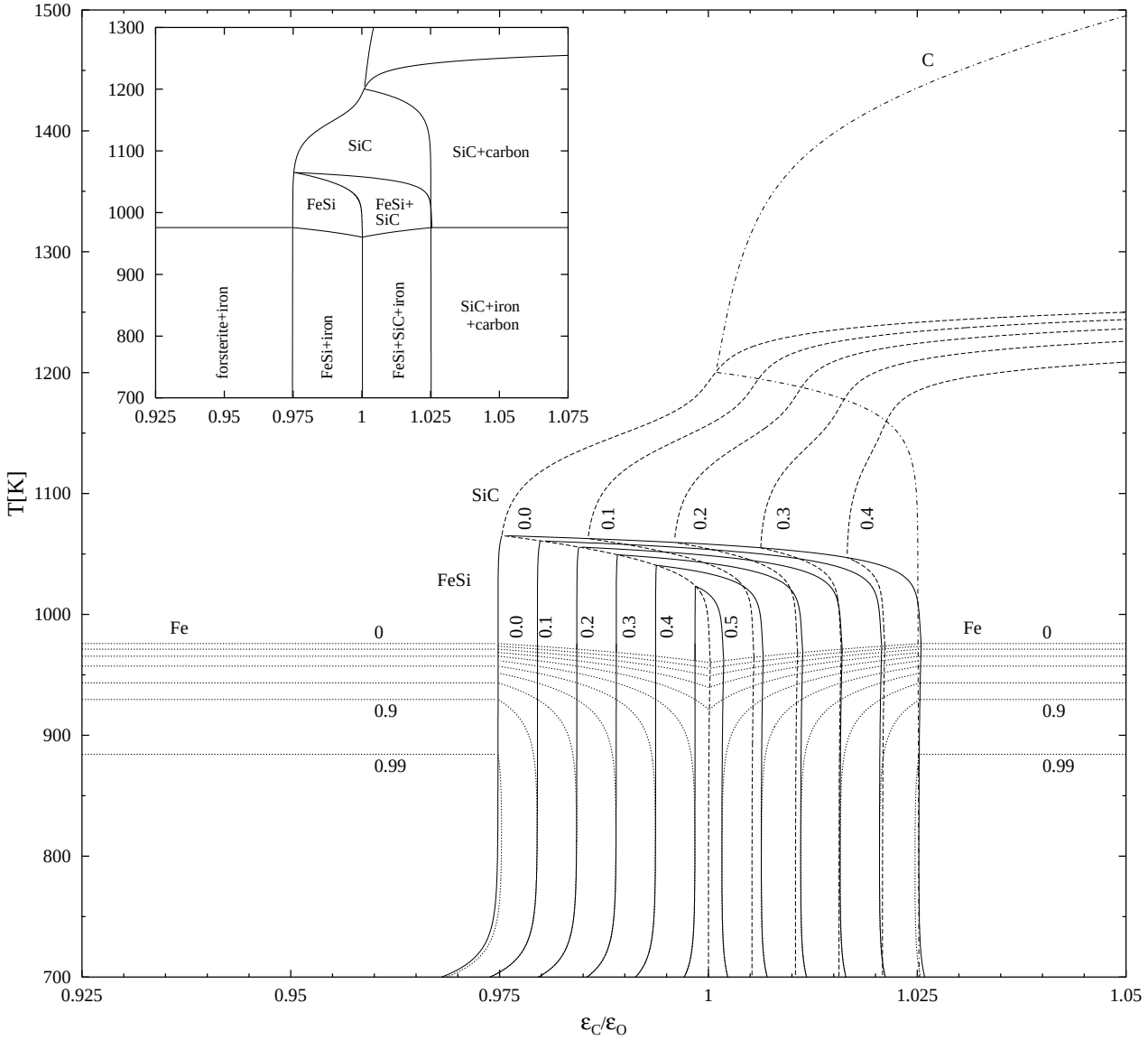

Fig. 4. Equilibrium condensation of FeSi (full line), solid iron (dotted line) and silicon carbide (dashed line) at $P = 10^{-4}\,\mathrm{dyn\,cm^{-2}}$ for varying C/O abundance ratios. The numbers at the lines denote the degree of condensation f of Fe in solid iron and FeSi and of Si in SiC, respectively. For iron $f = 0,\ 0.2, 0.4, 0.6, 0.8, 0.9$ and $f = 0.99$ is plotted. The dashed-dotted line labeled with C shows the stability limit of solid carbon. The inset in the left upper corner of the figure shows the different chemical equilibrium mineral mixtures and their regions of existence at the M–S–C transition.

in chemical equilibrium at low temperatures even in the carbon rich regime $\epsilon_C > \epsilon_{C,crit}$. This formation of silicates, if kinetically possible, would occur in the stellar wind in a region where condensation of silicates, carbon or any other dust material has already driven the wind to highly supersonic outflow velocities. The resulting rapid dilution of the wind material in this region and the resulting low particle densities makes it unlikely that formation of oxygen bearing solids by drawing oxygen from the CO reservoir really occurs.

4.2. Condensation of iron and iron compounds

The abundant iron is not incorporated into the silicates (except for a small fraction) as long as the temperature is well above 500 K and condensation occurs under equilibrium conditions (for the case of non-equilibrium condensation see Gail & Sedlmayr 1999). From the many studies of condensation sequences it is known that in chemical equilibrium the iron condenses as free metal. Figure 3 shows the upper stability limit of Fe for a typical pressure of $P = 10^{-4}\,\mathrm{dyn\,cm^{-2}}$ for varying carbon to oxygen ratios as dotted line. At the low pressures prevailing in circumstellar shells the condensation temperature is lower than that of the silicates. This condensation temperature does not depend on the carbon to oxygen abundance ratio as long as $\epsilon_C \lesssim \epsilon_{C,crit}$. Close to the critical carbon abundance $\epsilon_{C,crit}$ the condensation temperature of forsterite drops below that of iron because the freely available oxygen disappears from the gas phase.

At low temperatures the iron would be converted into FeS and in an oxygen rich environment also into iron oxides as has been shown in many calculations of condensation sequences. In Gail & Sedlmayr (1998a) it is shown that for kinetic reasons these conversions are unlikely to occur under circumstellar conditions. For this reason we do not consider FeS and iron oxides.

4.3. Condensation in the transition regime between $\epsilon_{C,crit}$ and $\epsilon_C \approx 1.025\epsilon_O$

In the region of carbon abundances between the critical carbon abundance $\epsilon_{\rm C,crit}$ and a carbon abundance slightly in excess of the oxygen abundance, the chemistry is characterised by the lack of both oxygen and carbon to form the silicates characteristic for M star dust shells and the soot characteristic for C star dust shells. Figure 4 shows the condensates formed from the most abundant refractory elements in this region of carbon to oxygen abundance ratios. These are: iron, silicon carbide, and iron silicide.

In our chemical equilibrium condensation calculations we have included some compounds which are not included in the previously published condensation calculations, even not in the extensive set of solids listed in Fegley & Lodders (1994). One group of compounds tested for their capability to condense in circumstellar dust shells was FeSi, $FeSi_2$, and Fe_3Si_7. We found that for a carbon abundance exceeding $\epsilon_{\rm C,crit}$ iron silicide FeSi is more stable in chemical equilibrium than the pure iron metal. The possible existence of this solid condensate for the element mixture in S stars has not been recognised in the past. We have recently shown, that this solid material is likely to exist in in circumstellar shells of stars with peculiar element abundances and detached dust shells by identifying some of the far infrared absorption bands of FeSi with observed but up to now not identified solid material absorption bands (Ferrarotti et al. 2000). The possible existence of FeSi has recently already been found by Lodders & Fegley (1999) from condensation calculations for C star element mixtures.

Figure 4 shows the degree of condensation of the abundant dust components in chemical equilibrium for the carbon abundance domain $\epsilon_{\rm C,crit} \le \epsilon_{\rm C} \lesssim 1.025\epsilon_{\rm O}$. Solid carbon is not considered in this calculation since it is not an important condensate in this region (cf. Fig. 5 for carbon condensation). The figure shows solid FeSi to be a very abundant dust species. Its upper stability limit occurs where SiC starts to consume nearly all of the Si. Its condensation temperature is even higher than that of solid iron. The iron silicide does exist in chemical equilibrium only for carbon to oxygen abundance ratios typical for the SC stars and extreme S stars ($\epsilon_{\rm C}/\epsilon_{\rm O} \gtrsim 0.975$). This needs, however not to be true for non-equilibrium condensation.

The silicon carbide also starts to condense for carbon abundances $\epsilon_{\rm C} > \epsilon_{\rm C,crit}$ at temperatures above the stability limit of FeSi. For carbon abundances in the region $\epsilon_{\rm C,crit} < \epsilon_{\rm C} < \epsilon_{\rm O}$ it disappears again once FeSi becomes stable. Since the maximum degree of condensation of Si in SiC in chemical equilibrium is small in this region of carbon abundances, silicon carbide probably is not an important condensate in this region, if ever.

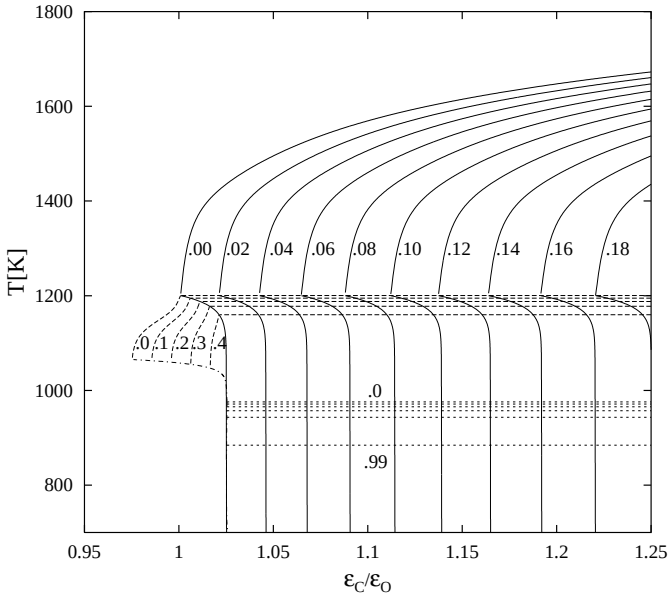

Fig. 5. Equilibrium condensation of carbon (full line), silicon carbide (dashed line), and iron (dotted line) at $P = 10^{-4}\,\mathrm{dyn\,cm^{-2}}$ for varying C/O–ratios. The numbers at the lines denote the degree of condensation f of C in solid carbon, of Si in solid SiC, and of Fe in iron, respectively. For iron $f = 0,\ 0.2, 0.4, 0.6, 0.8$ and $f = 0.99$ is plotted. The dashed-dotted line, the left lower, nearly horizontal line, shows the stability limit of solid FeSi (cf. Fig. 4).

For carbon abundances in the region $\epsilon_{\rm O} < \epsilon_{\rm C} \lesssim 1.025\epsilon_{\rm O}$ silicon carbide and iron silicide coexist in chemical equilibrium and it is possible that both dust species are formed in a circumstellar shell. This means that iron silicide dust may also be found in carbon stars with a very weak carbon excess.

For carbon abundances exceeding $\approx 1.025\epsilon_{\rm O}$ the iron silicide does not exist under chemical equilibrium conditions. In this region the iron condenses as the free metal, as in the oxygen rich region, while the silicon forms with carbon solid SiC.

Carbon becomes stable in chemical equilibrium if $\epsilon_{\rm C}/\epsilon_{\rm O} > 1$ at temperatures above the stability limit of silicon carbide (see Fig. 4, cf. also Fig. 5). In the region $1 < \epsilon_{\rm C}/\epsilon_{\rm O} \lesssim 1.025$ the carbon disappears again once SiC becomes stable. The fraction of the total carbon condensed into solid carbon is very small (cf. Fig. 5) and carbon is probably not an important dust component for SC stars with carbon to oxygen abundance ratios $1 < \epsilon_{\rm C}/\epsilon_{\rm O} \lesssim 1.025$.

The mixture of solids existing in the transition region between the oxygen rich and the carbon rich element mixture depends critically on the C and O abundances and

the temperature. In Fig. 4 we may distinguish eight regions where different mineral mixtures exist:

1. iron and forsterite;
2. iron and iron silicide;
3. iron, iron silicide, and silicon carbide;
4. iron, silicon carbide, and carbon;
5. iron silicide;
6. iron silicide and silicon carbide;
7. silicon carbide;
8. silicon carbide and carbon.

The regions of existence for varying C/O abundance ratios and temperatures at the transition from M to C stars for each of the different types of mineral mixtures are shown in the inset in the left upper corner of Fig. 4. This variety of possible mineral compositions makes S stars a particular interesting class of stars where very different types of dust mixtures may be found in their dust shells.

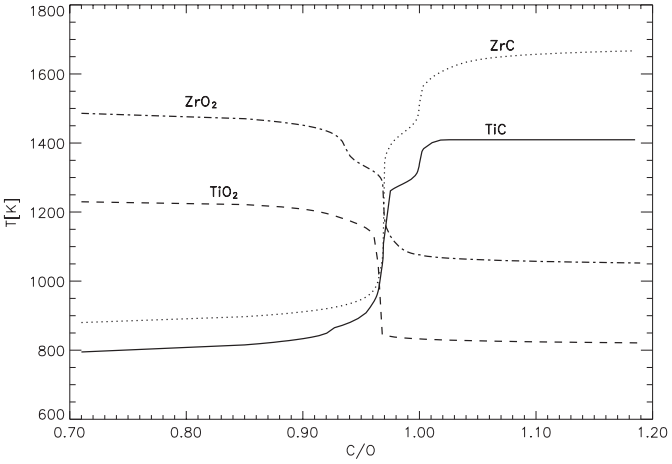

Fig. 6. Stability limits of some species which may be important for nucleation.

4.4. Condensation in the carbon rich regime

The carbon rich regime is characterised by the presence of a lot of carbon bearing molecules in the gas phase different from CO. As is well known, this requires $\epsilon_{\rm C} > \epsilon_{\rm O}$, which can also be seen by inspection of Fig. 1. At low temperature, the change in composition of the gas phase occurs rather abruptly at $\epsilon_{\rm C} = \epsilon_{\rm C,crit}$, as is shown in the two Figs. 1 corresponding to $T = 1000$ and $T = 1200\,{\rm K}$, respectively, and occurs more gentle at $\epsilon_{\rm C} = \epsilon_{\rm O}$ at higher temperatures, as is shown in Fig. 2 ($T = 2500\,{\rm K}$). Relevant for the problem of dust formation is the composition at low temperatures, while the composition at higher temperatures is what one sees in the stellar spectrum.

Figure 5 shows the degree of condensation of the abundant refractory elements into solids in the carbon rich region, as calculated for chemical equilibrium. The abundant dust species for this domain of C/O abundance ratios are solid carbon, SiC, and iron. Additionally MgS would condense at about 800 K (not shown in the figure and not discussed in this paper). The transition to a mixture characteristic for carbon rich material occurs at a carbon abundance of $\epsilon_{\rm C} \approx 1.025\epsilon_{\rm O}$ and not at $\epsilon_{\rm C} = \epsilon_{\rm O}$. If the carbon abundance of a star falls into the interval $\epsilon_{\rm O} < \epsilon_{\rm C} \lesssim 1.025\epsilon_{\rm O}$ the dust composition may be different from that expected for a C star though the stellar spectrum would look like that of a carbon star.

In this paper we do not consider the problem of dust formation in true carbon stars.

5. Nucleation

Though it is not our intention to discuss the problem of dust nucleation in this paper, we give some crude estimations on the possibility that seed nuclei for dust growth are formed from less abundant elements than those forming the dust seen as circumstellar dust. Figure 6 shows for the particular stable solid oxides and carbides of titanium and zirconium, which become stable already at rather high temperatures, the dependence of the stability limits on the C/O abundance ratio (cf. also Lodders & Fegley 1995). The abundance of Zr in Fig. 6 is already increased by a factor of 10 over its standard cosmic abundance to allow for the increased abundance of *s*-process elements after the onset of third "dredge-up". The figure demonstrates, that at the oxygen rich side ($\epsilon_{\rm C} < \epsilon_{\rm C,crit}$) the oxides of Zr and Ti are stable up to a much higher temperature than the silicates, while at the carbon rich side the carbides of Zr and Ti are stable up to higher temperatures than solid C and SiC at least for not too high carbon abundances. We do not consider the case $\epsilon_{\rm C} > 1.025\epsilon_{\rm O}$ of true carbon stars (for this case see e.g. Lodders & Fegley 1995, 1997, 1999). For S stars at the carbon rich side the carbides of Ti and Zr are stable up to a much higher temperature than the possible abundant condensates (Fe, FeSi, SiC). Thus, except for a very narrow transition region of the C/O abundance ratio at $\epsilon_{\rm C} = \epsilon_{\rm C,crit}$, solid compounds of Ti and Zr may form seed nuclei for the growth of the more abundant dust species. However, even with its increased abundance Zr seems not to be a likely candidate for seed particle formation, but the abundance of Ti is sufficiently high for this to be possible.

For carbon grain growth it is known from laboratory investigations of pre-solar dust grains (Bernatowicz et al. 1996) that at least in some instances carbon grains grow around seed nuclei of TiC or (Zr,Mo)C. In Gail & Sedlmayr (1998b) it is proposed that in an oxygen rich environment dust growth may occur on seed nuclei of TiO_2. On the basis of a simple model for the properties of TiO_2 clusters it was shown that TiO_2 nucleation occurs at a temperature of about 50 K above the stability limit of silicates. More detailed calculations based on quantum mechanical calculations of structures and bond energies of TiO_2 clusters have confirmed this (Jeong 2000).

Here we give a brief discussion of the possibility of formation of TiO_2 seed nuclei in the oxygen rich element mixture. We consider the problem of growth of TiO_2 clusters. If the growth does not start until the outflowing gas has

cooled sufficiently in order that a significant supersaturation ratio with respect to gas phase TiO_2 has developed, the equation for the growth of TiO_2 clusters is

$$\frac{\mathrm{d}a}{\mathrm{d}t} = V_0\, n_{\mathrm{TiO_2}} v_{\mathrm{th}}\, \alpha\,. \tag{5}$$

a is the grain radius and $n_{\mathrm{TiO_2}}$ the particle density of TiO_2 molecules. The volume occupied by TiO_2 in the solid is

$$V_0 = \frac{A_{\mathrm{TiO_2}}\, m_{\mathrm{H}}}{\rho_{\mathrm{TiO_2}}}. \tag{6}$$

$A_{\mathrm{TiO_2}} = 79.87$ is the molecular weight of TiO_2 and $\rho_{\mathrm{TiO_2}} = 4.23\,\mathrm{g\,cm^{-3}}$ the mass density of the solid. $v_{\mathrm{th}} = 3.2 \times 10^4\,\mathrm{cm\,s^{-1}}$ is the random mean square thermal velocity of TiO_2 molecules and α is the sticking coefficient which is assumed to be unity, because already the monomer is a tri-atomic molecule. The time required to grow to some prescribed radius a_{sn} of the seed nucleus is

$$t_{\mathrm{gr}} = a_{\mathrm{sn}} \left| \frac{\mathrm{d}a}{\mathrm{d}t} \right|^{-1}. \tag{7}$$

If this growth has to occur over a distance Δr corresponding to a change ΔT in temperature of the wind material, we have

$$\frac{\Delta r}{r} = 2\frac{\Delta T}{T} \tag{8}$$

since the temperature varies approximately as $T(r) \propto r^{-1/2}$ (grey temperature distribution). With $\Delta T \approx 50\,\mathrm{K}$, the temperature difference between nucleation of TiO_2 and the stability limit of the silicates, $T \approx 1000\,\mathrm{K}$, $r \approx 4.5\ R_* \approx 10^{14}\,\mathrm{cm}$ we have $\Delta r \approx 1 \times 10^{13}\,\mathrm{cm}$. The time available for seed particle growth is

$$t_{\mathrm{hydr}} = \frac{\Delta r}{v}. \tag{9}$$

The flow velocity v prior to the onset of rapid acceleration due to condensation of the abundant dust species should be of the order of the sound velocity $v \approx 10^5\,\mathrm{cm\,s^{-1}}$. Then $t_{\mathrm{hydr}} \approx 10^8\,\mathrm{s}$. This is the time available for seed particle growth.

In order that $t_{\mathrm{gr}} < t_{\mathrm{hydr}}$ we must have

$$n_{\mathrm{TiO_2}} \geq \frac{a_{\mathrm{sn}}}{V_0 v_{\mathrm{th}} \alpha t_{\mathrm{hydr}}}. \tag{10}$$

For a seed nucleus containing, for instance, 1000 TiO_2 molecules we have $a_{\mathrm{sn}} = 10 V_0^{\frac{1}{3}} = 3 \times 10^{-7}\,\mathrm{cm}$. Then we require $n_{\mathrm{TiO_2}} \geq 3 \times 10^3\,\mathrm{cm^{-3}}$. This is the minimum particle density of TiO_2 molecules required for efficient seed particle growth.

The number density of hydrogen nuclei in a stationary wind is

$$N_{\mathrm{H}} = \frac{\dot{M}}{4\pi m_{\mathrm{H}}} \frac{1}{r^2 v} \tag{11}$$
$$= 3 \times 10^{10} \left(\frac{\dot{M}}{10^{-5}\,M_\odot\,\mathrm{yr^{-1}}} \right) \left(\frac{10^{14}\ \mathrm{cm}}{r} \right)^2 \left(\frac{\mathrm{km\,s^{-1}}}{v} \right).$$

At a temperature of $\approx$1000 K the titanium is almost completely bound in TiO_2 molecules for the oxygen rich mixture. With the abundance given in Table 1 we have $n_{\mathrm{TiO_2}} \approx 3 \times 10^3\,\mathrm{cm^{-3}}$. Comparing this with our preceding condition $n_{\mathrm{TiO_2}} \geq 3 \times 10^3\,\mathrm{cm^{-3}}$ we conclude, that growth of seed nuclei of TiO_2 containing at least 10^3 monomeres is possible if $\dot{M} \gtrsim 10^{-5}\,M_\odot\,\mathrm{yr^{-1}}$ and growth of very small seed nuclei with at least 10 monomeres, which corresponds to clusters with 30 atoms, if $\dot{M} \gtrsim 2\,10^{-6}\,M_\odot\,\mathrm{yr^{-1}}$.

Thus, in the oxygen rich ($\epsilon_{\mathrm{C}} < \epsilon_{\mathrm{C,crit}}$) element mixture the formation of the abundant dust components is preceded by the formation and growth of TiO_2 clusters. These may serve as growth centres for the condensation of the abundant dust components. For seed nuclei formed from ZrO_2 the situation is less favourable because of the lower abundance of Zr, but for the highest mass loss rates $\dot{M} \gtrsim 10^{-5}\,M_\odot\,\mathrm{yr^{-1}}$ also seed particles from zirconium oxide may form in the stellar wind.

A discussion of the possible formation of TiC seed nuclei in the carbon rich mixture is given by Chigai, Yamamoto & Kozasa (1999), a possible observational identification of TiC clusters is discussed in von Helden et al. (2000).

6. Non-equilibrium condensation

The considerations on equilibrium condensation in Sect. 4 show which dust species are the most stable ones for stars with the peculiar element composition of AGB stars at the transition between M and C stars. Now we have to consider the problem which dust species are formed under the non-equilibrium conditions encountered in stellar outflows. In such outflows the dynamical expansion time-scale usually is shorter than the time-scale required for establishing chemical equilibrium. The chemistry, then, lags behind the change in the equilibrium composition towards which the chemical system tries to evolve and from some point on the density in the wind is so small that the chemistry is effectively frozen in. The dust composition obtained in such circumstances represents some transient state of the chemical evolution of the system, the nature of which can only be determined by solving the rate equations for dust growth in a cooling and expanding environment. It is to be expected, that the most stable equilibrium condensates also in this case are the dominating dust species, but the relative quantities of the different dust species formed under non-equilibrium conditions may be very different from what is found for the case of equilibrium condensation, cf. Paper II. In the following we present the basic equations for dust growth for the special conditions encountered for nearly equal abundances of oxygen and carbon and for the new dust species formed at the M-S-C transition.

6.1. Growth of silicate dust grains

The silicates forsterite and enstatite cannot condense directly from the gas phase by formation of their own seed

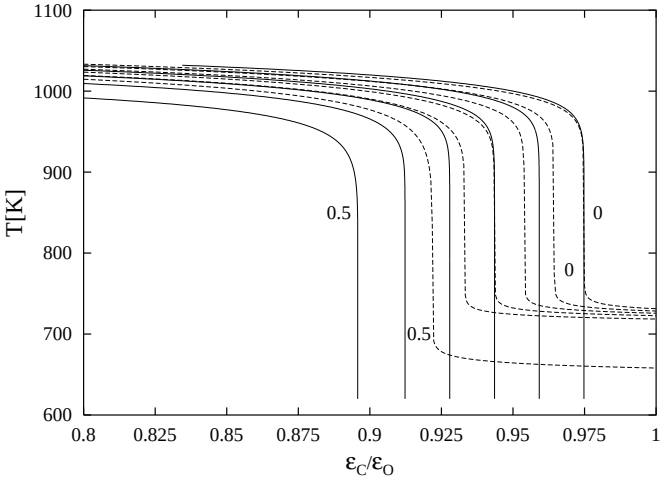

Fig. 7. Pseudo-equilibrium condensation of forsterite (full line) and enstatite (dashed line) at $P = 10^{-4}\,\mathrm{dyn\,cm^{-2}}$ for varying C/O abundance ratios, if each of the two solids could condense independently of the other one. The degree of condensation f of Si in the solids varies from $f = 0$ to $f = 0.5$ in steps of 0.1.

nuclei. Their growth from the gas phase requires the existence of some kind of pre-formed seed particles. These may be provided, for instance, by TiO_2 particles at the oxygen rich side of the M–S–C transition, as discussed in the preceding section. We leave open the precise nature of the seed nuclei, since this is presently not known, but merely assume that such particles do exist. For growth on pre-formed seed nuclei there usually exists no, or no significant, nucleation barrier and we assume that the silicates start to grow once the temperature in the outflow falls short of the stability limit of the bulk condensate.

In an oxygen rich element mixture the two most abundant solid condensates are olivine and pyroxene. Figure 3 shows the degree f of condensation of these two silicates (with $x = 1$) in chemical equilibrium, when they are nearly iron-free. For increasing carbon abundance condensation of enstatite is suppressed in the region of C/O abundance ratios typical for S stars because of the lack of available oxygen, which is completely bound in CO and forsterite, once the carbon abundance has increased to $\epsilon_C > \epsilon_O - 2\epsilon_{Mg}$. The suppression of enstatite formation needs, however, not to be true in a non-equilibrium situation. The stability limits of forsterite and enstatite for condensation from the gas phase are close to each other for a carbon to oxygen abundance ratio exceeding 0.8, as can be seen from Fig. 7 which shows the (pseudo-)equilibrium condensation of the two silicates calculated for the two hypothetical cases that only one of the silicates is allowed to condense, either forsterite or enstatite.

Since the stability limits of both silicates are very close in temperature, in a cooling outflow they both may start to condense on seed nuclei at nearly the same time and, as long as the condensible material in the gas phase is not yet strongly depleted by growth of the two solids, they grow independently from each other from the gas phase. Strong acceleration of the wind due to radiation pressure following the condensation of abundant and efficiently absorbing dust species then rapidly dilutes the wind material and prevents the system from evolving to the chemical equilibrium state. Thus, as discussed in Paper II, in a non-equilibrium condensation calculation one has to retain both silicates, even if an equilibrium calculation predicts one of them to be absent. The same holds for the formation of quartz, as was shown in Paper II. Thus we also have to consider the formation of quartz.

The non-equilibrium condensation of olivine and pyroxene has been considered in Paper II. In the present case there arises the problem that in the region of C/O abundance ratios typical for S stars and temperatures of the order of 1000 K or below, most of the oxygen is bound in CO and SiO (cf. top of Fig. 1). The growth of silicates then is limited by the fact that insufficient amounts of O are available in the gas phase to supply the oxygen required for complete condensation of Si into forsterite or enstatite. The growth rate in the oxygen rich case is determined by the collision rate with SiO molecules (see Paper I). The additional oxygen required to form the SiO_4–tetrahedrons in silicates is provided by H_2O molecules, which in the oxygen rich case are available in sufficient amounts from the gas phase. Also Mg and Fe are available in sufficient amounts from the gas phase. This is not valid for S stars where addition of oxygen probably becomes the rate limiting step. The most abundant O bearing species in the gas phase besides CO and SiO is H_2O for all carbon abundances $\epsilon_C < \epsilon_{C,crit}$ (cf. top of Fig. 1). Thus, formation of the basic building block SiO_4 of the silicate lattice requires for each SiO molecule to incorporate three (olivine) or two (pyroxene) additional H_2O molecules from the gas phase for supplying the required oxygen. Thus we assume as a working hypothesis that the growth rate for olivine J_{ol}^{gr} is given by

$$J_{ol}^{gr} = \begin{cases} J_{SiO} & \text{if } J_{H_2O} > 3J_{SiO} \\ \frac{1}{3}J_{H_2O} & \text{if } J_{H_2O} < 3J_{SiO} \end{cases} \tag{12}$$

and the growth rate of pyroxene J_{py}^{gr} is given by

$$J_{py}^{gr} = \begin{cases} J_{SiO} & \text{if } J_{H_2O} > 2J_{SiO} \\ \frac{1}{2}J_{H_2O} & \text{if } J_{H_2O} < 2J_{SiO} \end{cases} . \tag{13}$$

where

$$J_{SiO} = \alpha_{SiO} n_{SiO} v_{th,SiO} \tag{14}$$

$$J_{H_2O} = \alpha_{H_2O} n_{H_2O} v_{th,H_2O}. \tag{15}$$

The α's are the growth coefficients, for which we assume that $\alpha_{SiO} = \alpha_{H_2O}$. For α_{SiO} we use for olivine and pyroxene the values discussed in Paper II. With this assumption on the growth rates the radius change of silicate grains, the fractional contents x of magnesium in the lattice of olivine and pyroxene, and the consumption of condensible species from the gas phase are calculated as described in Papers I & II. Diffusion of Fe cations in the olivine and pyroxene lattice is not considered in the present paper.

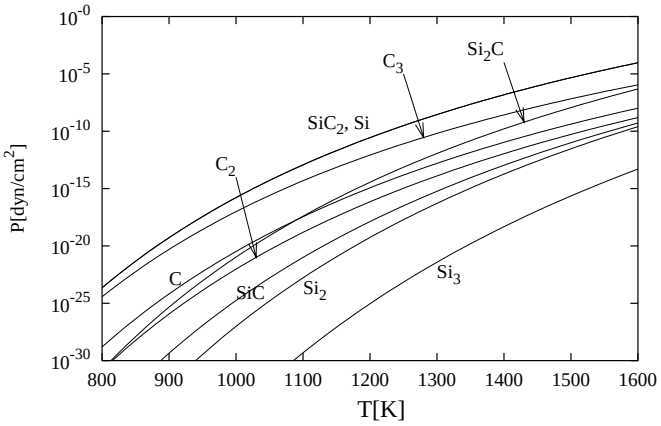

Fig. 8. Molecular composition of the vapour of SiC in chemical equilibrium.

With respect to the growth of quartz grains we assume that the growth rate is given by

$$J_{\rm qu}^{\rm gr} = \begin{cases} J_{\rm SiO} & \text{if } J_{\rm H_2O} > J_{\rm SiO} \\ \\ J_{\rm H_2O} & \text{if } J_{\rm H_2O} < J_{\rm SiO} \end{cases} . \tag{16}$$

For α we assume, again, that $\alpha_{\rm SiO} = \alpha_{\rm H_2O}$ and use the growth coefficient $\alpha_{\rm SiO}$ for quartz discussed in Paper II.

6.2. Growth of silicon carbide dust grains

Silicon carbide (or carborundum) dust grains are present in most carbon stars (cf. Wallerstein & Knapp 1998) as can be seen by the 11.3 μm emission feature of SiC, but they are absent from oxygen rich objects. Silicon carbide is also observed to be present in a small number of S stars (Chen & Kwok 1993). This seems quite natural in view of the dependence of the equilibrium abundance of SiC on the C/O ratio in the region of carbon to oxygen abundance ratios $\epsilon_{\rm C,crit} \lesssim \epsilon_{\rm C} \lesssim \epsilon_{\rm O}$ where typically S stars do appear. Figure 4 shows that at most 20% of the silicon may condense into SiC in chemical equilibrium, but only above the stability limit of FeSi. Once the latter becomes stable, SiC becomes unstable against conversion into FeSi. This does not exclude the formation of some quantities of silicon carbide in a non-equilibrium situation but it is unlikely that significant amounts of SiC will form in such a situation.

In the region $\epsilon_{\rm O} \lesssim \epsilon_{\rm C} \lesssim 1.025\epsilon_{\rm O}$ the chemical equilibrium abundance of SiC rapidly increases with increasing C/O ratio while the equilibrium abundance of FeSi drops to zero. Though silicon carbide is the stable Si bearing condensate only at C/O abundances where the star would be classified as C star, it seems likely that in a non-equilibrium situation for abundances close to or close above the limit $\epsilon_{\rm C} = \epsilon_{\rm O}$, where a star still may be classified as being of spectral type S, already a non negligible quantity of silicon carbide is formed. For this reason we include SiC condensation in our calculation of non-equilibrium dust formation.

Growth of silicon carbide from the gas phase is a process of technical interest for semiconductor fabrication, which has attracted much interest. For a recent discussion of this aspect with many references to the literature see Råback (1999). Such technical growth processes, however, are run under conditions different from that encountered in circumstellar shells in two respects: temperatures applied in the laboratory are much higher than in the condensation zone of circumstellar shells, and usually in technical processes silicon carbide is grown in a hydrogen poor environment. This makes the direct application of data for SiC growth in the laboratory to SiC growth in circumstellar shells somewhat questionable. Since no other sort of information on SiC growth seems to be available we nonetheless use this information for a preliminary calculation of SiC growth in circumstellar shells.

The sublimation growth of SiC has successfully been modelled by Råback (1999) by assuming a sticking coefficient α for vapour deposition of unity. Therefore we assume in our model calculation $\alpha = 1$.

Figure 1 shows that in the circumstellar shell there are essentially three potentially important gas phase species which may contribute to the growth of solid SiC at temperatures around $T = 1000\,$K: Si, Si_2C, SiC_2, and C_2H_2. The most abundant Si and C bearing species in the gas phase are SiC_2 and Si_2C within the temperature region between 1200 and 1000 K where the growth of SiC is expected to occur in a circumstellar shell (cf. top and middle of Fig. 1). SiC_2 dominates at higher temperatures while Si_2C dominates at lower temperatures. Since both, Si_2C and SiC_2, also are very abundant species in the gas phase under conditions of sublimation growth of SiC (cf. Råback 1999), we assume that growth of SiC occurs via deposition of one Si and one C atom to the surface of the growing crystal during collision with Si_2C or SiC_2 from the gas phase

$$J_{\rm SiC}^{\rm gr} = \left(n_{\rm Si_2C}\, v_{\rm Si_2C} + n_{\rm SiC_2}\, v_{\rm SiC_2}\right)\, \alpha\,, \tag{17}$$

where $n_{\rm SiC_2}$, $n_{\rm Si_2C}$ and $v_{\rm SiC_2}$, $v_{\rm Si_2C}$ are the particle densities and the rms. thermal velocities of the growth species, respectively.

The vapour composition during SiC sublimation can be obtained as follows: the vapour may be composed of Si, Si_2, Si_3, C, C_2, C_3, SiC, Si_2C, SiC_2, ..., from which, however, only Si and SiC_2 are really abundant (Note that the composition of the vapour of solid SiC is different from the mixture of Si-bearing molecules in the stellar wind). From the stoichiometric condition $p_{\rm Si} = p_{\rm SiC_2}$ and from the condition of chemical equilibrium between the solid and the gas

$$p_{\rm Si} p_{\rm C}\, {\rm e}^{-\Delta G/RT} = 1 \tag{18}$$

(ΔG being the free enthalpy of formation of solid SiC from the free atoms) and from the law of mass action

$$p_{\rm SiC_2} = p_{\rm Si} p_{\rm C}^2\, K_{\rm p}({\rm SiC_2})\,, \tag{19}$$

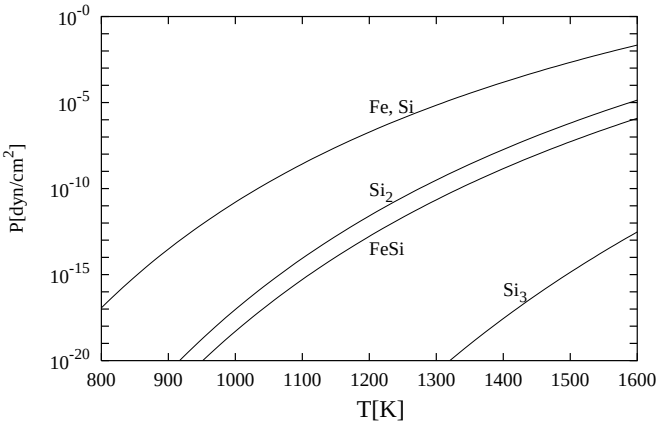

Fig. 9. Molecular composition of the vapour of FeSi in chemical equilibrium.

where K_p denotes the mass-action constant of SiC_2, one obtains in good approximation

$$p_\mathrm{C} = (K_\mathrm{p}(\mathrm{SiC_2}))^{-\frac{1}{2}} \quad , \quad p_\mathrm{Si} = \mathrm{e}^{\Delta G/RT} p_\mathrm{C}^{-1} \, . \tag{20}$$

The partial pressures of the other molecules are readily calculated from this. The resulting vapour composition of solid SiC is shown in Fig. 8. Since the dominating species in the vapour are SiC_2 and Si, the decomposition rate of solid SiC is

$$J_\mathrm{SiC}^\mathrm{dec} = 2\alpha v_{\mathrm{SiC_2}} \frac{p_{\mathrm{v,SiC_2}}}{kT} \, , \tag{21}$$

where $p_{\mathrm{v,SiC_2}}$ is the equilibrium vapour pressure of SiC_2 molecules. The factor of two accounts for the fact that injection of one SiC_2 into the gas phase is accompanied by the injection of one Si into the gas phase for stoichiometric reasons. By the loss of one SiC_2 from solid SiC two nominal molecules of SiC are lost from the solid.

The radius change of SiC grains (abbreviated as "sc") then is calculated from

$$\frac{\mathrm{d}a_\mathrm{sc}}{\mathrm{d}t} = V_{0,\mathrm{sc}} \left(J_\mathrm{sc}^\mathrm{gr} - J_\mathrm{sc}^\mathrm{dec} \right) \, . \tag{22}$$

This together with the rates (17) and (21) is our model for the growth of SiC grains. Equation (22) is solved from that point on where $J_\mathrm{sc}^\mathrm{gr} > J_\mathrm{sc}^\mathrm{dec}$.

The growth of SiC grains in C stars is discussed from a somewhat different point of view also by Kozasa et al. (1996).

6.3. Growth of FeSi dust grains

FeSi is unstable against conversion into solid Fe and silicon-oxygen compounds in the presence of H_2O. Therefore FeSi does not form for $\epsilon_\mathrm{C} < \epsilon_\mathrm{C,crit}$, as can be seen from Fig. 4. Its formation is possible only at the carbon rich side of the M-S-C transition.

Assuming spherical grains the equation of change for the grain radius of FeSi grains (abbreviated as "fs") is

$$\frac{\mathrm{d}a_\mathrm{fs}}{\mathrm{d}t} = V_{0,\mathrm{fs}} \left(J_\mathrm{fs}^\mathrm{gr} - J_\mathrm{fs}^\mathrm{dec} \right) \tag{23}$$

where $V_{0,\mathrm{fs}}$ is the volume occupied by one nominal molecule in the solid and $J_\mathrm{fs}^\mathrm{gr}$ and $J_\mathrm{fs}^\mathrm{dec}$ are the rates at which Si atoms are added to or removed from the surface of the solid per unit surface area by growth and decomposition processes, respectively.

The vapour composition of FeSi is calculated as follows: The vapour resulting from FeSi vapourisation is composed of free Fe and Si atoms and of the molecules FeSi, Si_2, and Si_3, from which only Fe and Si are really abundant. The stoichiometric conditions then require that we have $p_\mathrm{Fe} = p_\mathrm{Si}$. Chemical equilibrium between the vapour and the solid requires

$$1 = p_\mathrm{Fe} p_\mathrm{Si} \, \mathrm{e}^{-\Delta G/RT} \, , \tag{24}$$

where ΔG is the free enthalpy of formation of solid FeSi from the free atoms. From these two conditions one obtains the approximation (with very good accuracy)

$$p_\mathrm{Fe} = p_\mathrm{Si} = \mathrm{e}^{\Delta G/2RT} \, . \tag{25}$$

From this the vapour pressures of the different molecules can be calculated. Figure 9 shows the vapour composition of FeSi. It is composed nearly exclusively of free Fe and Si atoms, justifying our assumption on which the approximate solution (25) is based. The decomposition rate of FeSi then can be calculated from

$$J_\mathrm{fs}^\mathrm{dec} = \alpha_\mathrm{FeSi} v_{\mathrm{th,Si}} \frac{p_{\mathrm{v,Si}}}{kT} . \tag{26}$$

The vapour pressure $p_{\mathrm{v,Si}}$ is given by (25). We have not succeeded to find measured values for the vapourisation coefficient of FeSi. Since FeSi behaves at high temperatures like a metal, we assume a coefficient $\alpha_\mathrm{FeSi} = 1$ typical for metals.

Abundant Fe and Si bearing species in the stellar wind for oxygen to carbon abundance ratios typical for S stars are (cf. top of Fig. 1)

Fe, Si, SiO, SiS, Si_2C .

A possible growth mechanism for FeSi is the addition of Fe and Si atoms from the gas phase. The rate determining step in this case is the addition of Si atoms, since in the wind material they are less abundant than Fe atoms (cf. Fig. 1). The growth rate then is

$$J_\mathrm{fs}^\mathrm{gr} = \alpha_\mathrm{FeSi} v_{\mathrm{th,Si}} n_\mathrm{Si} \, . \tag{27}$$

For the three alternative reactions

$$\mathrm{Fe} + \mathrm{SiO} \rightarrow \mathrm{FeSi(s)} + \mathrm{O}$$

$$\mathrm{Fe} + \mathrm{SiS} \rightarrow \mathrm{FeSi(s)} + \mathrm{S}$$

$$\mathrm{Fe} + \mathrm{Si_2C} \rightarrow \mathrm{FeSi(s)} + \mathrm{SiC}$$

the change of free enthalpy ΔG is $+41$, -131, -336 kJ Mol^{-1}, respectively (data from Barin 1992). The formation of FeSi(s) from Fe atoms and SiO is not possible, but formation from Fe and SiS or Si_2C in principle could occur but is not considered in our model calculation.

Equations (23), (26), and (27) define our model assumption for the growth of FeSi grains in circumstellar shells of s stars. The growth Eq. (23) is solved from that point on where $J_\mathrm{fs}^\mathrm{gr} > J_\mathrm{fs}^\mathrm{dec}$.

6.3.1. Possibility of direct nucleation of FeSi

Inspection of Fig. 1 shows that the gas phase abundance of FeSi molecules at $T = 1000\,\mathrm{K}$ is low, but not extremely low. They certainly are not important for FeSi growth, but they may be responsible for direct nucleation of FeSi from the gas phase by homogeneous nucleation if no other suited seed nuclei for FeSi grains are available. If the critical cluster for nucleation is the monomer FeSi, we obtain for the nucleation rate (cf. Gail & Sedlmayr 1998a)

$$J_{\mathrm{nucl}} = n_{\mathrm{FeSi}}^2 v_{\mathrm{th,FeSi}} \sigma \alpha\,. \tag{28}$$

For estimating the order of magnitude of the nucleation rate we use $v_{\mathrm{th}} = 3 \times 10^4\,\mathrm{cm\,s^{-1}}$, $\sigma = 10^{-15}\,\mathrm{cm^2}$, $\alpha = 1$, $n_{\mathrm{FeSi}}/N_{\mathrm{H}} = 10^{-10}$ (cf. Fig. 1) and obtain for the number of grains formed per hydrogen nucleus and per second

$$\frac{J_{\mathrm{nucl}}}{N_{\mathrm{H}}} \approx 3 \times 10^{-31} N_{\mathrm{H}}. \tag{29}$$

For the number density of H nuclei we have

$$N_{\mathrm{H}} = \frac{\dot{M}}{1.4 m_{\mathrm{H}}\, 4\pi\, r^2 v}. \tag{30}$$

Since FeSi will be the first strong absorbing material condensing in the wind of S stars, only a substantial condensation of FeSi drives the wind to highly supersonic velocities, provided the wind of S stars is driven by dust condensation and not by some completely different mechanism (like pulsation). Then we can assume that the wind enters the dust forming zone around the star with a slightly subsonic velocity, for instance with $v_{\mathrm{gas}} \approx 10^5\,\mathrm{cm\,s^{-1}}$. A temperature of $T \approx 1000\,\mathrm{K}$ is reached at $r \approx 4.5\,R_* \approx 1 \times 10^{14}\,\mathrm{cm}$ for a star with $L = 10^4\,L_\odot$ and $T_{\mathrm{eff}} = 3000\,\mathrm{K}$. The density of hydrogen nuclei then is $n_{\mathrm{H}} \approx 3 \times 10^{10}\,\mathrm{cm^{-3}}$. If we arbitrarily assume that the extension of the dust forming layer is of the order of $0.5\,R_*$, the residence time of the wind material in the dust forming layer is

$$\tau_{\mathrm{gr}} = \frac{\Delta r}{v_{\mathrm{gas}}} \approx 1 \times 10^8\,\mathrm{s}\,. \tag{31}$$

The number of FeSi dust grains formed in the wind by direct FeSi nucleation follows as

$$\frac{n_{\mathrm{gr}}}{N_{\mathrm{H}}} = \frac{J_{\mathrm{nucl}}}{N_{\mathrm{H}}} \tau_{\mathrm{gr}} \approx 9 \times 10^{-13}\ \frac{\mathrm{grains}}{\mathrm{H\text{-}nucleus}}\,, \tag{32}$$

which is of the right order of magnitude to allow for efficient condensation in the wind.

This estimate refers to the rather extreme situation of a strong supercooling when the size of the critical cluster for nucleation has dropped to the monomer, which seems unlikely to occur under realistic conditions. It shows, however, that FeSi could, at least in principle, be formed directly from the gas phase without the requirement of preformed seed nuclei. A nucleation of FeSi in condensation experiments using shock tubes is reported to be observed by Stephens (1989). Since in the stellar outflow centres for heterogeneous growth on seed nuclei are likely to exist, we assume in our model calculations that FeSi grows on pre-formed seed nuclei.

Table 3. Data used in the calculation of growth and vapourisation rates.

Dust species	A	ρ	α	Reference
$(Mg,Fe)_2SiO_4$	172.23	3.75	0.1	Nagahara & Ozawa (1996)
$(Mg,Fe)SiO_3$	116.16	3.58	0.1	estimate
Fe	55.85	7.86	1.0	Landolt-Börnstein (1968)
FeSi	83.93	6.1	1.0	estimate
SiC	40.10	2.2	1.0	Råback (1999)

6.4. Growth of iron dust grains

Figure 4 shows that solid iron is a possible condensate in the region of C/O abundance ratios relevant for S stars. Different from the case of M and S stars, however, this is not the only stable Fe bearing condensate but part of the Fe will condense into FeSi.

Nucleation of iron grains from the gas phase is not possible because of the low bond energy in small iron clusters (Gail & Sedlmayr 1998a). Iron can be formed only by heterogeneous growth on some of the seed nuclei formed above the condensation temperature of Fe. The formation of pure iron grains does not depend on the carbon to oxygen abundance ratio in the stellar outflow since, independent of the C/O abundance ratio, the only abundant Fe bearing gas phase species is the free Fe atom. The only difference to the case of iron condensation in true M and C stars is that for S stars Fe formation occurs in competition with FeSi formation. The growth of iron grains is calculated as in Papers I & II.

6.5. Carbon condensation

In chemical equilibrium small amounts of carbon dust may condense if the carbon to oxygen abundance ratio exceeds ≈1.025 (cf. Fig. 5). Such stars will be assigned the spectral type C and not spectral type S according to the molecular abundances in their stellar atmosphere (cf. Fig. 2). At C/O abundance ratios below ≈1.025 no condensed carbon exists in chemical equilibrium.

Carbon growth occurs in circumstellar dust shells under non-equilibrium conditions (e.g. Cherchneff 1998). Though carbon becomes thermodynamically stable in carbon rich element mixtures at temperatures above 1400 K (see Fig. 5) the basic processes of carbon growth from a hydrogen-acetylene gas mixture do not work at temperatures above ≈1100 K (e.g. Cherchneff 1998). Carbon dust then does not form at a much higher temperature than the other abundant dust species. Since only small quantities of carbon dust can be formed at carbon overabundances up to $\mathrm{C/O} \lesssim 1.05$ they are dynamically not significant compared to the radiative acceleration of the wind by the other dust species. For this reason we do not consider carbon dust formation in this paper.

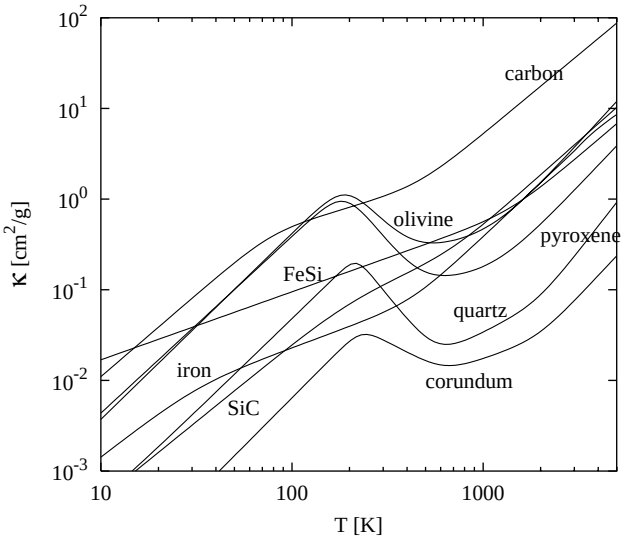

Fig. 10. Rosseland mean opacities for different dust materials of interest for circumstellar shells of S stars, assuming a MRN grain size distribution. The mass extinction coefficient corresponds to complete condensation of the respective key elements into the dust species.

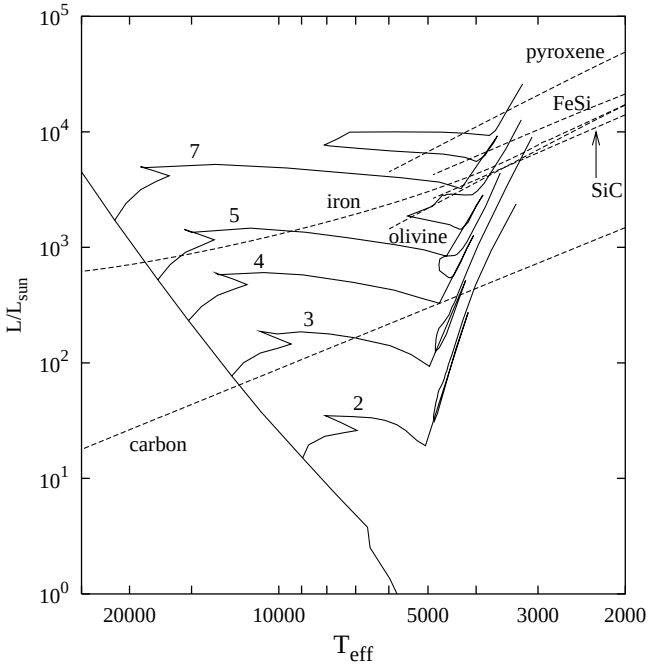

Fig. 11. Eddington limit luminosities $L_{\rm edd}$ for some important dust materials are shown as dotted lines. Above this limit radiation pressure on grains of the indicated dust species is able to drive a stellar wind. The limit luminosity is calculated for a stellar mass of $M_* = 1\,M_\odot$ and a degree of condensation of the respective key element of $f = 0.5$. For other fractional condensations and stellar masses the limit luminosity scales as M_*/f. For comparison, some evolutionary tracks in the HR-diagram for stars with initial stellar masses between 2 and $7\,M_\odot$ (Meader & Meynet 1988) are shown as full lines.

7. Model calculation

7.1. Wind model

We have calculated simple models for the condensation of dust in the outflow from stars with varying carbon to oxygen abundance ratios from C/O < 1 to C/O > 1 in order to study the compositional changes of the circumstellar dust during the M-S-C transition.

The stationary, spherically symmetric wind model on which these calculations are based on is described in Paper II. With respect to the details of the model calculation for the stellar outflow we refer to that paper.

The chemical composition of the gas phase is calculated by assuming chemical equilibrium for the molecular species. The calculation is restricted to a subset of the most abundant molecules of the elements H, C, N, O, Mg, Si, Fe, S, Al, and Ca. For the dust growth problem the abundances of H_2O, SiO, Si, SiS, SiC_2, Si_2C, Fe, and Mg are of particular importance. The assumption of chemical equilibrium seems to be somewhat critical with respect to the abundances of Si, Si_2C, and SiC_2 in the region $\epsilon_{\rm C} \approx \epsilon_{\rm C,crit}$, since in this region these particular molecular species are minor species (cf. Fig. 1), whose abundance in a real stellar outflow may be somewhat different from their chemical equilibrium abundances. A non-equilibrium calculation of such species would be desirable, but the reaction kinetics of the Si_mC_n compounds seems not to be well known.

The equations of dust growth for olivine, pyroxene, quartz, iron, FeSi, and SiC are described in the preceding paragraph and Papers I + II. They are solved for each of the dust species from that point on outwards, where the growth rate first exceeds the decomposition/vapourisation rate of the dust species. The sticking coefficients used for calculating the growth of the different dust components are listed in Table 3. For integrating the growth equations for the olivine and pyroxene we have to specify the exchange coefficient $\alpha_{\rm ex}$ for Mg and Fe (defined in Paper I). This determines to a large extent the ratio Fe/(Mg+Fe) of the silicates. Unfortunately this quantity is poorly known (see Paper I) and we use in the present calculation a value of $\alpha_{\rm ex} = 0.1\alpha$ where α is the sticking coefficient for grain growth. This low value results in a high Fe/(Mg+Fe) ratio of the grains, essentially equal to that in the gas phase (≈0.4, if part of the Fe is bound in iron grains). A side effect of a low $\alpha_{\rm ex}$ and the resulting high iron content of olivine and pyroxene is a reduction of their condensation temperature as compared to their iron free counterparts forsterite and enstatite (cf. Fig. 1 of Paper I, for instance). Observationally it is known that the silicate dust component in circumstellar shells, if its lattice structure is crystalline, is nearly iron free (Molster 2000). The problem of formation of a crystalline dust component and its iron content is out of the scope of the present paper, we only consider formation of amorphous silicate dust.

The extinction coefficient κ is calculated as in Paper II by a simple superposition of the extinction coefficients κ

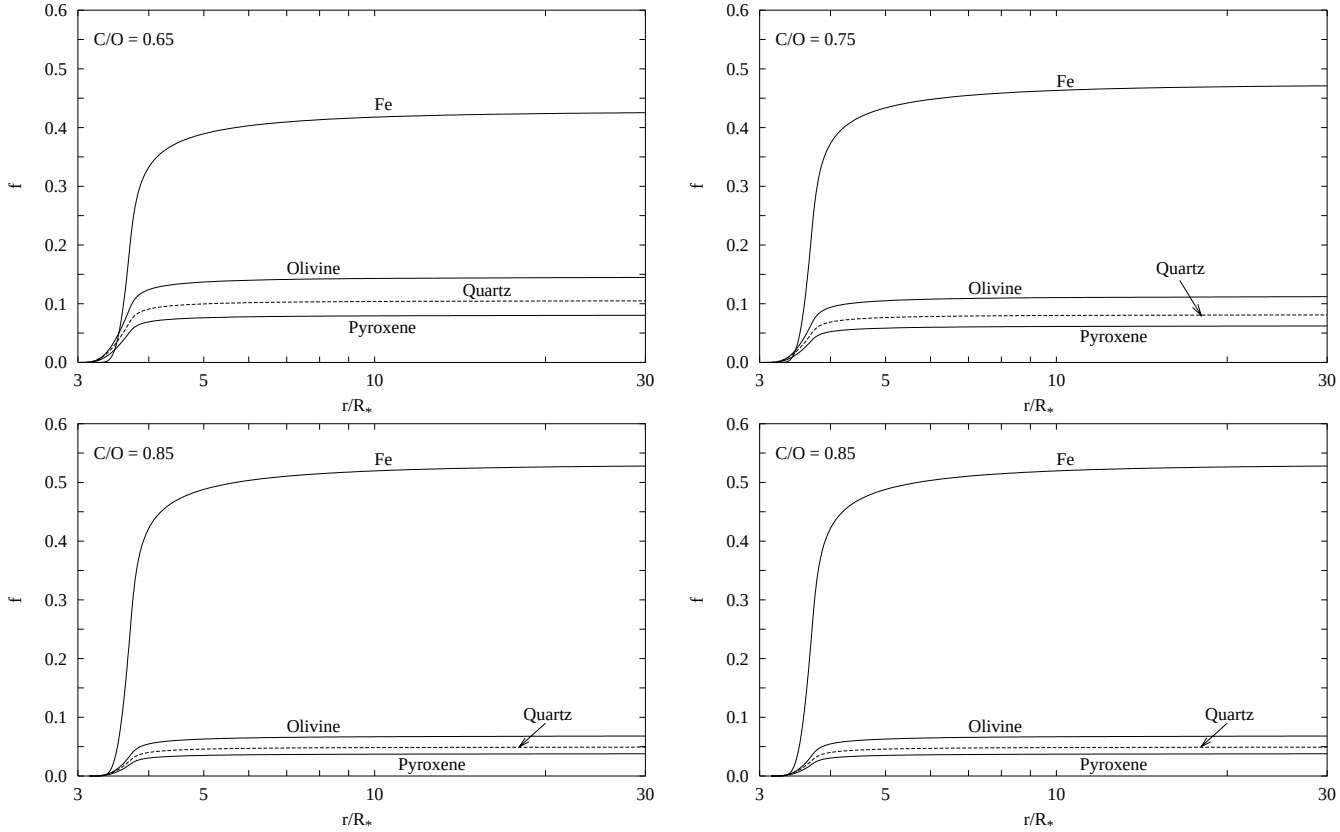

Fig. 12. Degree of condensation f of the dust species formed in M and S stars for some C/O abundance ratios at the oxygen rich side $\epsilon_{\rm C} < \epsilon_{\rm C,crit}$ of the chemical composition. The degrees of condensation f refer to the fraction f of the totally available Si condensed into olivine, pyroxene, or quartz, and to the fraction f of the totally available Fe condensed into solid iron. The wind model is calculated for a mass-loss rate of $\dot{M} = 10^{-5}\,M_\odot\,{\rm yr}^{-1}$. Metallic iron, olivine, quartz, and pyroxene are the dominant dust species in the circumstellar shells of S-stars with atmospheric abundances where they spectroscopically would be classified as MS or S-stars. Closer to the limit $\epsilon_{\rm C} = \epsilon_{\rm C,crit} \approx 0.975\epsilon_{\rm O}$ iron grains are the dominating dust species.

of the different dust species and of the of gas

$$\kappa = f_{\rm ol}\kappa_{\rm ol} + f_{\rm py}\kappa_{\rm py} + f_{\rm Fe}\kappa_{\rm Fe} + f_{\rm FeSi}\kappa_{\rm FeSi} + f_{\rm SiC}\kappa_{\rm SiC} + \kappa_{\rm mol} \quad (33)$$

$\kappa_{\rm ol}$ ... are the mass extinction coefficients of the different dust species, calculated for complete condensation of the key element in the dust species, and $f_{\rm ol}$ ... are the fractions of the key elements really condensed into the grains. These are calculated from the solution of the equations of grain growth analogously as it is described in Paper II. For Fe, FeSi, and SiC we use the optical constants described in Appendix A and calculated Rosseland-averaged mass extinction coefficients as described in Paper I. The results for SiC and FeSi are rather accurately fitted by

$$\kappa_{\rm SiC}(T) = \left[\frac{1}{(9.560\times10^{-6}T^{1.710})^4} + \frac{1}{(7.791\times10^{-4}T^{.8808})^4 + (1.171\times10^{-6}T^{1.879})^4}\right]^{-\frac{1}{4}}. \quad (34)$$

and

$$\kappa_{\rm FeSi}(T) = \left[\left(4.071\times10^{-3}\,T^{.6981}\right)^4 + \left(9.251\times10^{-7}\,T^{1.849}\right)^4\right]^{\frac{1}{4}}. \quad (35)$$

The gas opacity $\kappa_{\rm mol}$ is approximated by the fit formula for the Rosseland mean of the mass extinction by molecules as given by Bell & Lin (1994).

Figure 10 shows the Rosseland mean opacities of the dust components included in the model calculation and of some other dust components of interest for circumstellar dust shells. The dust extinction of the silicates are for amorphous dust grains. Figure 11 shows the Eddington limit luminosity

$$L_{\rm edd} = \frac{4\pi cGM_*}{f\kappa} \quad (36)$$

for different dust species and a representative degree of condensation of $f = 0.5$. $L_{\rm edd}$ defines the minimum luminosity required in order that radiation pressure on grains can drive a supersonic outflow. Note that silicates, Fe, and FeSi all are nearly equally efficient in driving a stellar wind.

The general properties of the wind models calculated are similar to that shown in, e.g., Paper I and will not be discussed further.

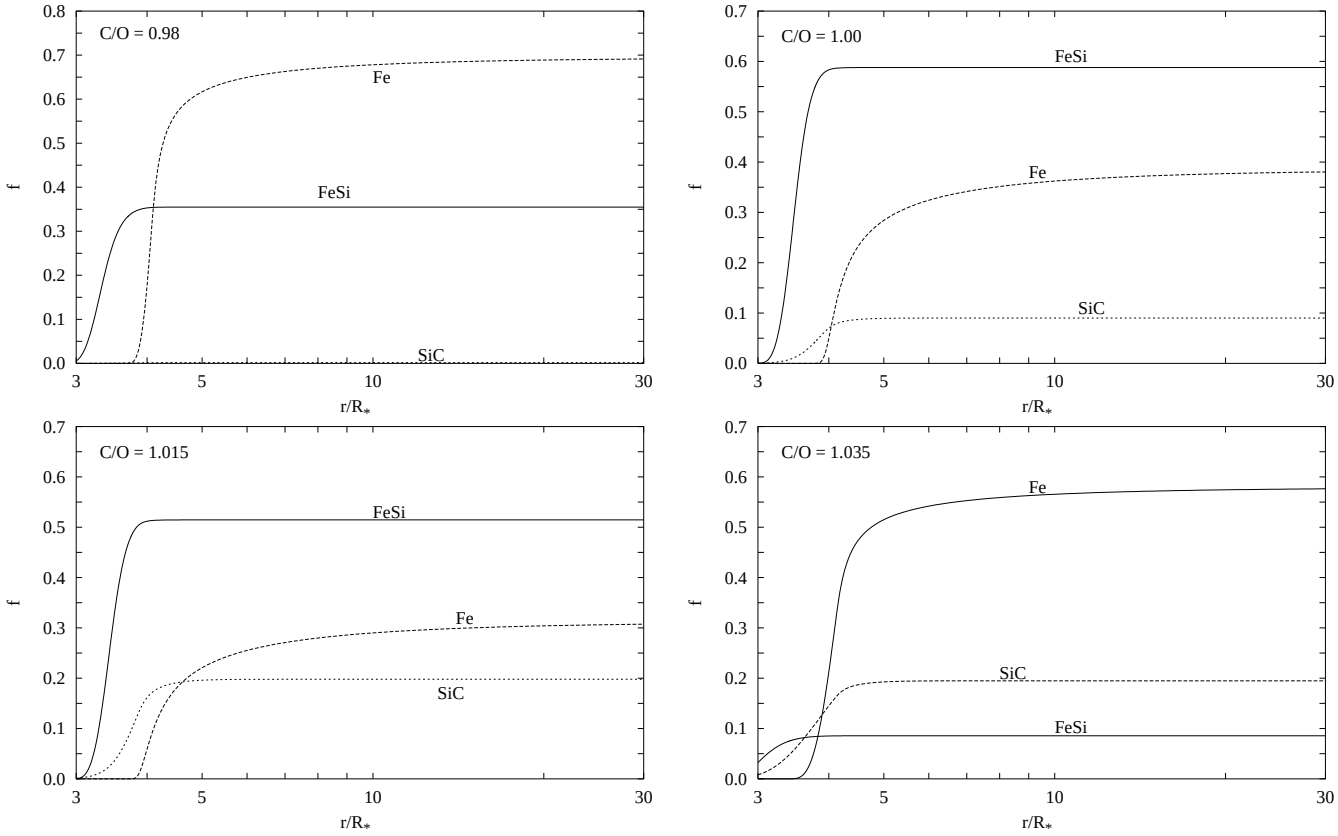

Fig. 13. Degree of condensation f of the dust species formed in S-stars for some C/O abundance ratios at the carbon rich side $\epsilon_{\rm C} > \epsilon_{\rm C,crit}$ of the chemical composition. The degrees of condensation f refer to the fraction f of the totally available Si condensed into SiC and FeSi, and to the fraction f of the totally available Fe condensed into dsolid iron. The wind model is calculated for a mass-loss rate of $\dot{M} = 10^{-5}\,M_\odot\,{\rm yr}^{-1}$. Iron and FeSi are the dominant dust species in the circumstellar shells of S-stars with atmospheric abundances where they would spectroscopically be classified as SC or even as S stars. SiC becomes an abundant dust species only for C stars with $\epsilon_{\rm C} > \epsilon_{\rm O}$.

7.2. Results for individual dust models

7.2.1. Dust condensation in S stars

For carbon to oxygen abundance ratios less than the critical value $\epsilon_{\rm C,crit}/\epsilon_{\rm O} = 0.975$ the most abundant dust species expected from chemical equilibrium calculations to be formed in the dust shell are silicates and solid iron. The dust mixture, then, essentially equals that of normal M stars.

Figure 12 shows the result of non-equilibrium dust formation calculations for the radial variation of the fraction of the Si condensed into the different silicate dust species and the fraction of the Fe condensed into iron grains for some selected values of the C/O abundance ratio. The wind models in this Fig. are calculated for a mass-loss rate of $\dot{M} = 10^{-5}\,M_\odot\,{\rm yr}^{-1}$. Obviously, the abundance of the silicate dust components decreases with increasing carbon abundance because the abundance of the H_2O vapour required for the further oxidation of the SiO added to the solid becomes scarce. At the same time the fraction of iron dust formed in the wind gradually increases because the abundance of the growth species for iron, the free Fe atom, does not depend on the C/O abundance ratio. The decrease of the available oxygen slows down the silicate growth with increasing C/O abundance ratio up to the point where for sufficiently high C/O ratio radiation pressure on iron grains already drives the outflow to highly supersonic velocities. In this case the rapid dilution of the wind material additionally inhibits the growth of silicate grains.

The non-TE calculation shows that a certain fraction of quartz is formed. This fraction is somewhat higher than what we have found in Paper II, because we assume in this paper a lower value for the exchange coefficient $\alpha_{\rm ex}$. This low value increases somewhat the fraction of quartz formed in a non-TE calculation, since a high iron content of olivine and pyroxene lowers their condensation temperature and brings it closer to the condensation temperature of quartz. Since quartz, then, starts to form already before the acceleration of the wind by radiation pressure on olivine and pyroxene strongly dilutes the outflowing gas, the quartz grains have chance to collect a bigger fraction of the available SiO as compared to the case where quartz condensation starts only after already significant olivine and pyroxene formation has taken place.

7.2.2. Dust condensation in SC stars and weak carbon stars

The chemical equilibrium condensation calculations indicate a drastic change in the chemical composition of the dust formed in the stellar outflow if the carbon abundance exceeds the critical value $\epsilon_{\rm C,crit}$ defined by (1). For $\epsilon_{\rm C,crit} < \epsilon_{\rm C} < \epsilon_{\rm O}$ the stars would be classified according to the appearance of their spectra as extreme S stars, for $\epsilon_{\rm O} < \epsilon_{\rm C} \lesssim 1.1\epsilon_{\rm O}$ as SC stars and for $\epsilon_{\rm C} \gtrsim 1.1\epsilon_{\rm O}$ as C-stars (Jaschek & Jaschek 1987). The chemistry in the transition region $\epsilon_{\rm C,crit} < \epsilon_{\rm C} < \epsilon_{\rm O}$ is characterised by the non-availability of oxygen and carbon for the formation of solids. Solid iron and FeSi are the most stable condensates under these circumstances. At somewhat higher carbon abundances (C/O > 1) conditions become favourable for condensation of SiC.

Figure 13 shows results of model calculations of non-equilibrium dust formation for the radial variation of the degree of condensation for the dust components Fe, FeSi and SiC. The wind models are calculated assuming a mass loss rate of $\dot{M} = 10^{-5}\ M_\odot\,{\rm yr}^{-1}$ and four different C/O abundance ratios. The top left figure refers to an abundance $\epsilon_{\rm C} = 0.98\epsilon_{\rm O}$ which is very close to the critical abundance $\epsilon_{\rm C,crit} = 0.975$. Iron dust is the dominating dust species in this case and also some FeSi is formed. This changes rapidly if the C/O ratio only slightly increases the critical value $\epsilon_{\rm C,crit}/\epsilon_{\rm O} \approx 0.975$. FeSi then is the dominating dust species. Silicon carbide first appears in non-negligible amounts if the carbon abundance exceeds the oxygen abundance, as is expected from chemical equilibrium calculations. With further increase of the carbon abundance the fraction of the FeSi-dust decreases and the fraction of metallic iron dust increases, but FeSi does not disappear as an important dust component at $\epsilon_{\rm C}/\epsilon_{\rm O} = 1.025$, as the results of the equilibrium condensation suggests, but is formed in significant amounts even at higher C/O abundance ratios. This results from the fact that in the outflow due to rapid dilution of the wind material the chemical composition does not develop into a chemical equilibrium state. The mineral mixture in the outflow represents a frozen in transient state.

This result indicates that FeSi may not only be formed in S-stars but even in carbon stars.

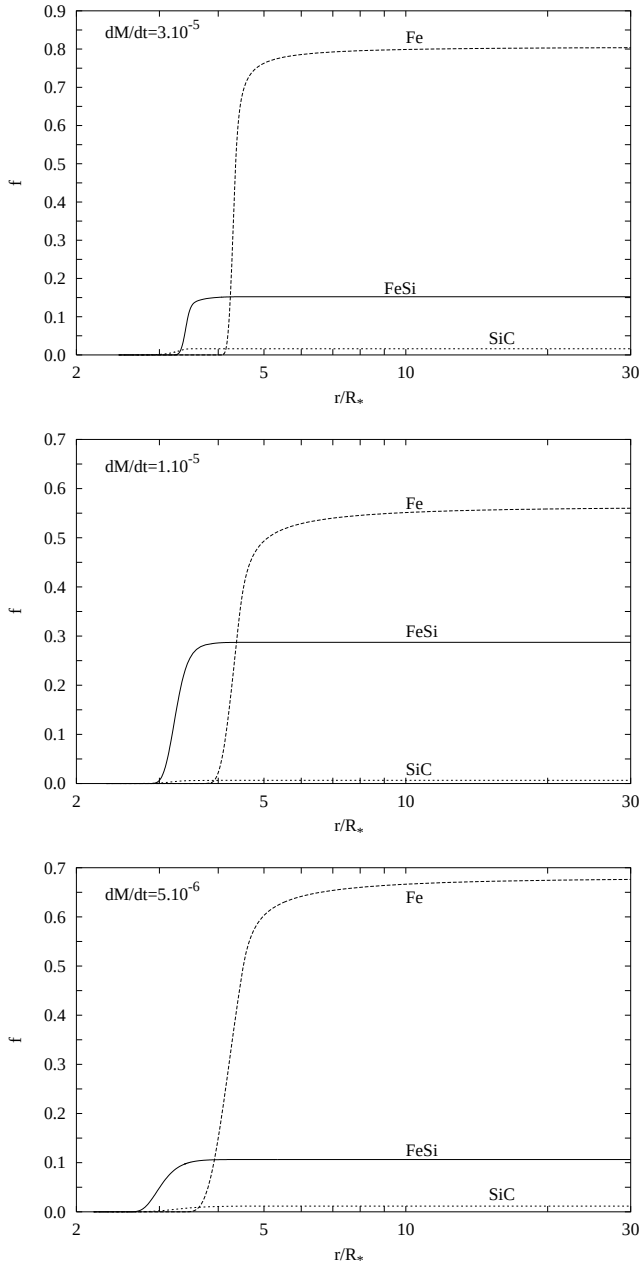

Fig. 14. Wind models for different mass-loss rates and a carbon to oxygen abundance ratio of $\epsilon_{\rm C}/\epsilon_{\rm O} = 1.00$. The degrees of condensation f refer to the fraction f of the totally available Si condensed into SiC and FeSi, and to the fraction f of the totally available Fe condensed into solid iron.

7.2.3. Dependence of dust condensation on the mass-loss rate

Figure 14 shows as an example the variation of the dust composition in the wind with varying mass-loss rate for the carbon rich side of the element mixture. The relative amounts of metallic iron and FeSi grains formed in the wind obviously depend strongly on the mass-loss rate. This results from the fact that (i) the rate determining step of FeSi growth is the addition of atomic Si and (ii) that free Si atoms are only a minor species at the low temperature where growth of Fe and FeSi grains is possible (cf. Fig. 1). This favours iron growth for low mass loss rates because, though FeSi starts to condense at a significantly higher temperature than Fe, the growth of FeSi is slower as that of metallic Fe and the degree of condensation of FeSi for low mass-loss rates does not reach the level required for strong wind acceleration before condensation of iron becomes possible. The rapid growth of iron from that point on then quickly forms sufficient amounts of condensed iron material so as to accelerate the wind to highly supersonic velocities by means of radiation pressure on iron grains. This in turn inhibits further growth

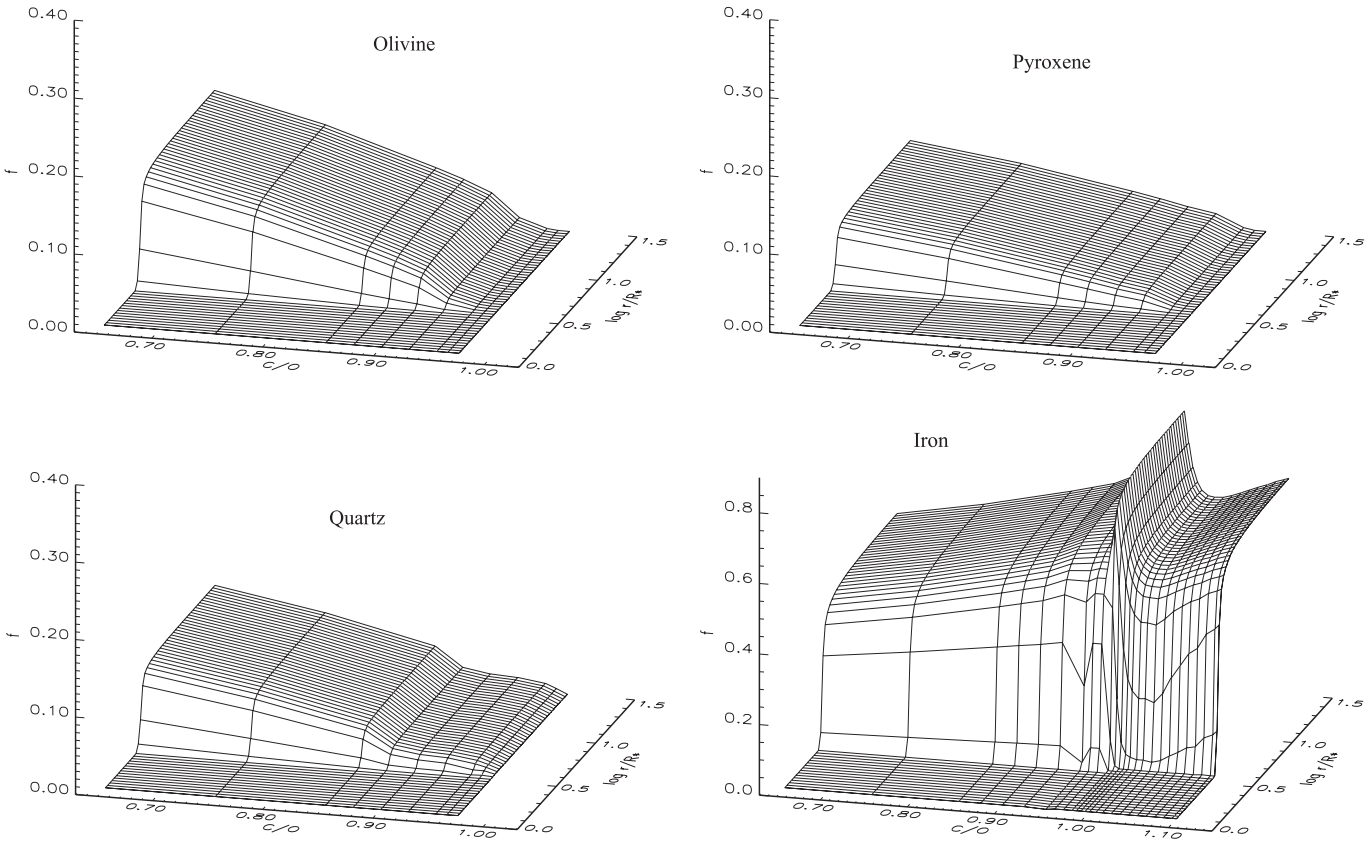

Fig. 15. Radial variation of the degree of condensation f for dust species at the oxygen rich side of the M-S-C transition and their dependence on the C/O abundance ratio. *Top left:* fraction of the Si condensed into olivine. *Top right:* fraction of the Si condensed into pyroxene. *Bottom left:* fraction of the Si condensed into quartz. *Bottom right:* fraction of the Fe condensed into metallic iron. The wind models are calculated for a mass-loss rate of $\dot{M} = 10^{-5}\ M_\odot\,\mathrm{yr}^{-1}$. Note that the f-scale for Fe is different from that for the Si-compounds.

of FeSi, which is the reason for the low abundance of FeSi in the high mass-loss model in Fig. 14.

For low mass-loss rates we, thus, expect as a result of non-equilibrium dust formation in the stellar outflow much iron dust to be formed but only low amounts of FeSi, though this should be the dominating dust species in the abundance region $\epsilon_{\mathrm{C,crit}} \lesssim \epsilon_{\mathrm{C}} \lesssim 1.025\epsilon_{\mathrm{O}}$. FeSi can be formed as an abundant dust species only in objects with a very high mass loss rate.

7.3. Change of dust composition at the M-S-C transition

The variation of the dust composition in the circumstellar dust shell is calculated for a set of models with C/O ratios ranging from C/O = 0.65 to C/O = 1.10. This covers the abundance range starting from stars which would appear as pure M stars according to their atmospheric spectra up to stars which appear as almost pure carbon stars. The composition of the dust mixture changes completely within a narrow C/O abundance interval around $\epsilon_{\mathrm{C,crit}}/\epsilon_{\mathrm{O}} = 0.9751$.

Figure 15 shows the results for the oxygen rich side of the abundance ratios. We have plotted the degree of condensation of Si into the Si bearing condensates olivine, pyroxene, and quartz, and of Fe into solid iron. Note that, additionally, part of the iron is condensed into olivine and pyroxene. As can easely be seen, the abundances of the silicate dust species olivine and pyroxene decrease with increasing C/O abundance. The main reason is the decrease in the abundance of H_2O in the gas phase which is required to oxidise the SiO from the gas phase to the SiO_4 building block of the silicates. This limits the growth velocity of olivine and pyroxene as the abundance ratio of C/O approaches $\epsilon_{\mathrm{C,crit}}/\epsilon_{\mathrm{O}}$ and suppresses their formation for $\epsilon_{\mathrm{C}} > \epsilon_{\mathrm{C,crit}}$. The growth of quartz also is limited by the lack of available oxygen. First its abundance significantly drops between the two limits given by (3) and (4) because the oxygen becomes scarce and mainly is consumed by forsterite and enstatite formation. The quartz vanishes as one approaches the limit $\epsilon_{\mathrm{C}} = \epsilon_{\mathrm{C,crit}}$, but less strongly than forsterite and enstatite. Close to the critical abundance ratio quartz according to our model calculation would be the dominating Si bearing dust species.

Parallel to the decrease of the silicate dust abundances the abundance of iron dust increases. The reasons for this are twofold. Firstly, Fe also is incorporated into the silicate dust. The fraction of the total Fe which can condense

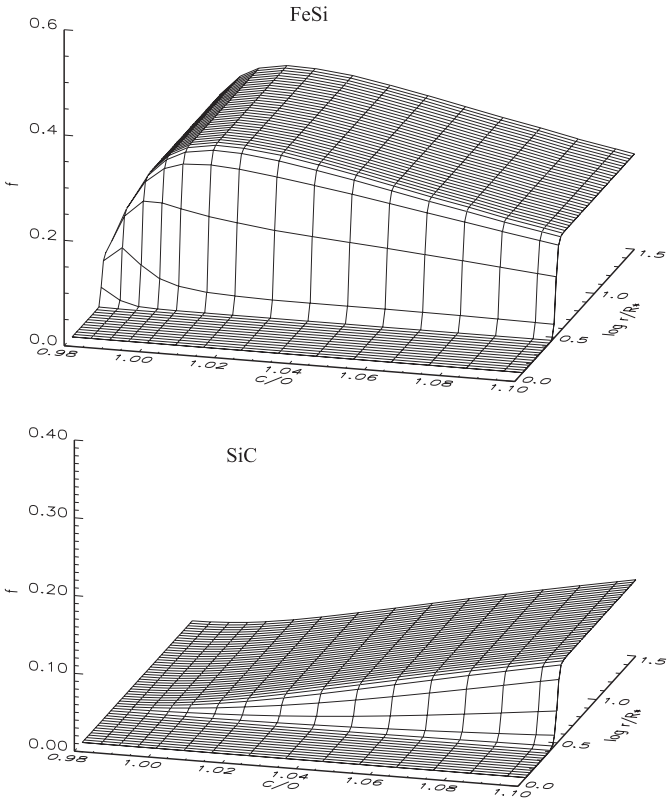

Fig. 16. Radial variation of the degrees of condensation f of Fe into solid FeSi and of Si into solid SiC and their dependence on the C/O abundance ratios at the carbon rich side of the M–S–C transition. The wind models are calculated for a mass-loss rate of $\dot{M} = 10^{-5}\,M_\odot\,\mathrm{yr}^{-1}$. Note that the f-scale for FeSi is different from that for SiC.

into iron dust grains therefore increases with decreasing silicate dust abundance. Secondly, with decreasing abundance of the oxygen not bound into CO the stability limit of the silicates decreases and at about $\epsilon_\mathrm{C} = 0.85\epsilon_\mathrm{O}$ drops below the stability limit of solid iron, which does not depend on the C/O abundance ratio. The rapid growth of iron prior to the onset of silicate condensation and the resulting radiation pressure on iron dust grains then drives the gas to high outflow velocities which hinders the growth of silicates by the rapid dilution of the gas. Close to the critical abundance $\epsilon_\mathrm{C} = \epsilon_\mathrm{C,crit}$ only iron dust is formed in the outflow with any noticeable abundance.

Figure 16 shows results for the carbon rich side of the CO abundance ratios. We have plotted the degree of condensation of Fe into FeSi and the degree of condensation of Si into SiC. The degree of condensation of Fe into iron grains is already shown in Fig. 15. Note the strongly stretched abscissa in Fig. 16. For carbon abundances $\epsilon_\mathrm{C} > \epsilon_\mathrm{C,crit}$ the fraction of Fe condensed into solid iron rapidly decreases in favour of the formation of solid FeSi. The FeSi appears for $\epsilon_\mathrm{C} > \epsilon_\mathrm{C,crit}$ because (i) with increasing C/O ratio only a decreasing fraction of the Si can be bound into the very strongly bound SiO molecule and (ii) the second most stable Si molecule, the SiS, cannot bind all the silicon because the sulphur abundance is only about one half of the silicon abundance. The excess of Si then is available to form FeSi, which is more stable than pure iron (cf. Fig. 4).

For $\epsilon_\mathrm{C} > \epsilon_\mathrm{O}$ the formation of significant amounts of SiC becomes possible. As Fig. 16 shows the degree of condensation of Si in SiC rapidly increases, once the C/O abundance ratio increases unity. At the same time the fraction of FeSi decreases again because the SiC condenses prior to FeSi and consumes the silicon required for the formation of FeSi.

The models are calculated up to a carbon abundance of $\epsilon_\mathrm{C} = 1.1\epsilon_\mathrm{O}$. This is probably higher than the C/O abundance ratio for which stars with the peculiar dust mixture of S stars exist, because at a C/O abundance ratio slightly in excess of unity carbon dust can be formed, which is not included in the present model calculation.

7.4. Infrared spectra

A set of synthetic spectra for wind models with $\dot{M} = 1 \times 10^{-5}\ M_\odot\,\mathrm{yr}^{-1}$ and a set of carbon to oxygen abundance ratios ranging from $\epsilon_\mathrm{C}/\epsilon_\mathrm{O} = 0.75$ to $\epsilon_\mathrm{C}/\epsilon_\mathrm{O} = 1.10$ have been calculated in order to explore the effects of the compositional variations of the dust mixture on the infrared spectrum emitted by the dust shell at the M-S-C transition. The oxygen abundance is held fixed and the carbon abundance is increased in steps of $\Delta\epsilon_\mathrm{C}/\epsilon_\mathrm{O} = 0.01$. The details of the radiative transfer calculation in the dust shell are described in Paper II. The optical constants used in the calculation for the oxygen rich models ($\epsilon_\mathrm{C} < \epsilon_\mathrm{C,crit}$) are the same as in Paper II, for the carbon rich models ($\epsilon_\mathrm{C} > \epsilon_\mathrm{C,crit}$) the optical constants of FeSi and SiC used in the calculation are described in Appendix A.

Figure 17 shows the synthetic infrared spectra. Figure 17a refers to the oxygen rich mixture ($\epsilon_\mathrm{C} < \epsilon_\mathrm{C,crit}$) where the dust in the circumstellar shell is a mixture of olivine, pyroxene, quartz, and iron. The dependence of the composition of the mixture on the oxygen to carbon abundance ratio can be seen from Fig. 15. One easely recognises the two silicate features characteristic for amorphous olivine and pyroxene centred at about 9.7 μm and 18 μm and two weak features from glassy quartz. The rather abundant iron dust component has no spectral features, it merely acts as a nearly grey background absorption. The silicate features are very pronounced up to a C/O ratio of 0.9 and then rapidly vanish, as also may be inferred from the degree of condensations shown in Fig. 15.

According to the present model calculation some quantities of quartz may be formed, which are responsible for two clearly visible solid state features centered around ≈8.7 and 20.6 μm. These features appear rather pronounced close to the critical abundance ratio $\epsilon_\mathrm{C}/\epsilon_\mathrm{O} = 0.975$, especially the feature around 20.6 μm. This results from the rather strong quartz feature and the fact that quartz disappears with increasing C/O abundance ratio as the last Si bearing dust component. Close to $\epsilon_\mathrm{C} = \epsilon_\mathrm{C,crit}$

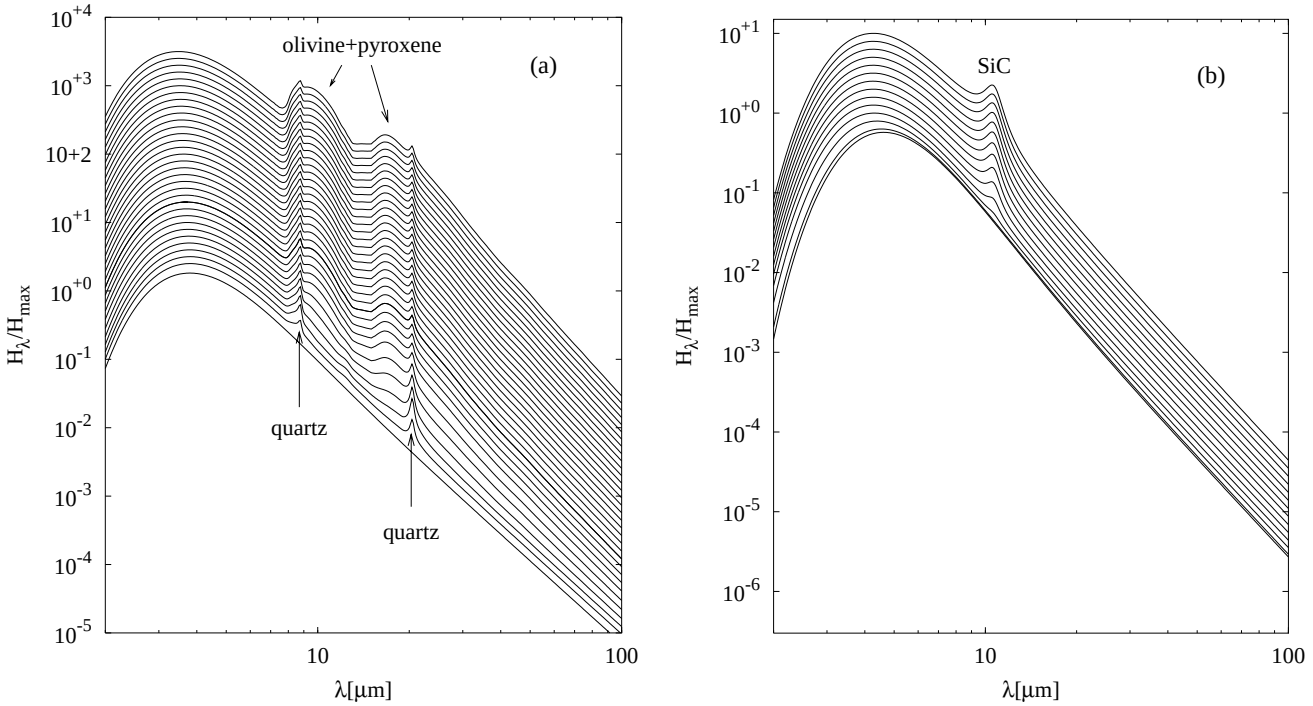

Fig. 17. Synthetic infrared spectra from circumstellar dust shells for different carbon to oxygen abundance ratios. **a)** Spectra for the oxygen rich side with C/O abundance ratios ranging in steps of $\Delta\epsilon_C/\epsilon_O = 0.01$ from $\epsilon_C/\epsilon_O = 0.65$ (uppermost spectrum) up to 0.96 and for the critical abundance $\epsilon_{C,crit}/\epsilon_O = 0.975$ (bottom) where $\epsilon_{C,crit}$ is defined by Eq. (1). The individual spectra are normalised to the maximum of H_λ and are shifted by a factor of $10^{0.1}$ each in the plot. **b)** The same at the carbon rich side for C/O ratios for $\epsilon_{C,crit}/\epsilon_O$ and from $\epsilon_C/\epsilon_O = 0.98$ (bottom) up to $\epsilon_C/\epsilon_O = 1.10$ (top). The spectra are calculated for wind models with a mass-loss rate of $\dot{M} = 1 \times 10^{-5}\ M_\odot\,\mathrm{yr}^{-1}$.

the quartz features are no more blended with the strong silicate features.

Figure 17b refers to the carbon rich mixture ($\epsilon_C > \epsilon_{C,crit}$) where the dust in the circumstellar shell is a mixture of solid iron, FeSi and SiC. The dependence of the composition of the mixture on the oxygen to carbon abundance ratio can be seen from Fig. 16. In this mixture only SiC has a pronounced absorption band centred at about 11.3 μm. The FeSi in principle also has some characteristic extinction bands in the far infrared spectral region (Ferrarotti et al. 2000) which, however, do exist only for very low temperatures $T \lesssim 200\,\mathrm{K}$ where FeSi behaves optically nearly like an insulator. For the circumstellar shell the dust is much warmer and FeSi then behaves optically like a metal. The absorption band due to SiC appears in the spectrum only for $\epsilon_C > \epsilon_O$. In the narrow region of C-abundances $\epsilon_{C,crit} < \epsilon_C \lesssim \epsilon_O$ where the star spectroscopically appears as a SC-star, nearly no SiC is formed in the outflow.

In the transition region between $\epsilon_C \approx 0.9\epsilon_O$ and $\epsilon_C \approx 1.02\epsilon_O$ the spectra appear as a practically featureless continuum. Such an absorption behaviour often is thought to result from the featureless extinction by carbon dust, but according to our model calculation this instead is the result of the featureless iron and FeSi extinction. The true S stars which neither are capable to form silicate dust nor to form carbon dust are nonetheless efficient dust factories, they form nearly pure iron dust or a mixture of iron and FeSi. The empirical observation of Jura (1988) that "grains around S stars are more similar to those around carbon-rich asymptotic giant branch stars than to the grains around oxygen-rich stars" now finds a simple explanation: it is the similarity of the infrared absorption properties of C, Fe, and FeSi (resulting from the fact that all three are electrically conductors) that mimics carbon-like absorption properties of dust around S stars.

7.5. Empirical mass-loss rates and dust to gas ratios

The dust-loss rates of S stars and their dust to gas mass-ratios have repeatedly been estimated (e.g. Groenewegen & de Jong 1998 and references therein) by a method proposed by Jura (1988), which relates the observed flux at 60 μm to the mass-loss rate. The results depend on the adopted value of the mass extinction coefficient at $\lambda = 60\,\mu$m, for which, following Jura (1988), generally a value of $\kappa(60\ \mu\mathrm{m}) = 150\,\mathrm{g\,cm}^{-2}$ corresponding to the mass absorption coefficient of graphite is assumed. Our results show, however, that the dust mixture around S stars is dominated by iron and in the carbon rich mixture by a mixture of Fe and FeSi. We find for the mass extinction

coefficients at $\lambda = 60\,\mu$m for these dust materials the following values:

$$\text{Fe: } 12.2\,\text{cm}^2\,\text{g}^{-1},\ \text{FeSi: } 21.5\,\text{cm}^2\,\text{g}^{-1},\ \text{C: } 145\,\text{cm}^2\,\text{g}^{-1}. \quad (37)$$

Iron and FeSi have lower extinction coefficients than carbon, cf. also Fig. 10. This means that the dust-loss rates determined in this way have to be increased by a factor between about 7 and 12, because the true emissivity of the dust material is lower than the assumed emissivity. The precise value of the correction depends on the C/O abundance ratio and can only be determined by modelling the dust shells. In any case, the correction brings dust-loss rates determined by this method for S stars closer to values determined for M or C stars. The same holds for the derived dust to gas mass-ratios, which has been claimed to be lower in S stars (e.g. Bieging & Latter 1994; Sahai & Liechti 1995) than in M or C stars.

8. Concluding remarks

We have considered the dust formation processes in circumstellar shells of AGB stars at the M-S-C-transition. From calculations of the chemical equilibrium mineral mixture for C/O abundance ratios between 0.65 and 1.1 we have found that solid iron and FeSi should be the dominating dust species in the circumstellar shells around S stars. This dust mixture is quite different from the dust mixtures usually observed to be formed in the circumstellar shells around M stars (olivine and pyroxene) and C stars (solid carbon and SiC).

We have developed a model for the non-equilibrium condensation of dust in the stellar wind of S stars. The mineral mixture obtained under non-equilibrium conditions is different from that predicted by chemical equilibrium calculations, but the dominating species formed in the wind are the same as in chemical equilibrium though in different relative amounts. The model calculations show that solid iron and FeSi are expected to be the most abundant dust species in dust shells around S stars.

Since for the warm dust observed to exist in the circumstellar dust shells of AGB stars both, Fe and FeSi, are electrical conductors, the infrared emission from this mixture should be characterised by a featureless continuum. According to the synthetic spectra we have calculated for our models of a stationary wind, the emission from dust around S stars should show no strong solid state absorption or emission bands, neither from silicates nor from SiC. This is in accord with the observational findings.

Despite the similarity of the infrared spectral energy distribution of S stars the extinction properties of the dust in S stars are different from that of carbon dust. The repeatedly applied method of Jura (1988) for determining dust-loss rates and to derive from this gas to dust ratios for S stars needs modification to account for the different extinction properties of dust in S stars. Mass loss-rates and gas to dust ratios will be somewhat higher than presently determined values.

Table A.1. Parameters of the Drude-Lorentz model for the optical constants of some dust materials.

ϵ_0	ω_j	ω_{pj}	γ_j
		SiC	
1	1.494×10^{14}	2.712×10^{14}	1.488×10^{13}
	1.991×10^{14}	2.247×10^{14}	4.092×10^{14}
	2.045×10^{16}	1.076×10^{16}	1.746×10^{15}
	1.752×10^{16}	1.418×10^{16}	4.627×10^{15}
		Fe	
1	0	1.175×10^{16}	2.853×10^{15}
	0	4.648×10^{15}	2.667×10^{13}
	3.752×10^{15}	1.155×10^{16}	3.761×10^{15}
	1.741×10^{16}	3.105×10^{16}	4.249×10^{16}
		FeSi	
2.212	0	8.374×10^{15}	3.852×10^{15}
	8.780×10^{11}	9.807×10^{14}	1.001×10^{14}
	2.045×10^{14}	5.211×10^{14}	1.148×10^{14}
	1.383×10^{15}	2.003×10^{15}	1.177×10^{15}
	3.643×10^{15}	7.158×10^{15}	3.958×10^{15}
	5.664×10^{15}	1.711×10^{16}	2.383×10^{16}
	6.684×10^{15}	7.735×10^{15}	3.945×10^{15}
	1.065×10^{16}	3.109×10^{15}	1.513×10^{15}
	1.461×10^{16}	4.953×10^{15}	4.304×10^{15}
	1.863×10^{16}	8.788×10^{15}	4.589×10^{15}

The quantitative results of the present model calculations depend critically on the adopted values of the growth efficiencies α, which are not always known with sufficient accuracy. The results for the wind models should, therefore, be considered only as a demonstration of what probably is going on in the dust formation zone of circumstellar shells around S stars.

Acknowledgements. This work has been performed as part of a project of the special research programme SFB 439 *"Galaxies in the Young Universe"* which is supported by the Deutsche Forschungsgemeinschaft (DFG).

Appendix A: Extinction by dust grains

The extinction efficiencies $Q_{\rm abs}$, $Q_{\rm sca}$ of dust grains are calculated from Mie theory for spherical grains (cf. Bohren & Huffman 1983). The optical constants n and k required for this are calculated from an analytical fit to experimental data for the optical properties of the different dust materials.

The complex dielectric constants ϵ of the dust materials are fitted with a Drude-Lorentz model. This model describes the variation of $\epsilon(\omega)$ with frequency ω as the superposition of a number of Lorentz profiles

$$\frac{\omega_{\rm p}^2}{\omega^2 - \omega_0^2 + i\gamma\omega} \quad (A.1)$$

Table A.2. Polynomial coefficients for calculating the free enthalpies of formation from free atoms for FeSi and NiSi molecules and for some Fe, Ni, and Si solid compounds. Units for ΔG are Kcal/Mole, pressures are in bar.

Compound	Phase	a	b	c	d	e
FeSi	gas	3.28729×10^{6}	-8.78894×10^{4}	5.44736×10^{1}	-1.59335×10^{-2}	3.54848×10^{-6}
NiSi	gas	6.38287×10^{6}	-1.07255×10^{5}	2.02338×10^{2}	-5.46060×10^{-3}	2.39700×10^{-6}
FeSi	sol	1.28292×10^{5}	-2.26646×10^{5}	7.49195×10^{1}	-1.68879×10^{-3}	-1.44677×10^{-7}
$FeSi_2$	sol	1.19491×10^{4}	-3.34623×10^{5}	1.11840×10^{2}	-4.23977×10^{-4}	-7.70794×10^{-7}
NiSi	sol	3.31257×10^{4}	-2.31096×10^{5}	7.38113×10^{1}	-1.63917×10^{-3}	1.41709×10^{-7}
Ni_7Si_{13}	sol	4.71476×10^{5}	-2.26229×10^{6}	7.38716×10^{2}	-1.94029×10^{-2}	1.69815×10^{-6}

resulting from damped oscillators with resonant frequency ω_0 and damping constant γ.

In the case of electrically conducting materials the contribution of the charge carriers to the complex dielectric constant can be represented by the Drude model

$$\frac{\omega_{\rm p}^2}{\omega^2 + i\gamma\omega}. \tag{A.2}$$

Here $\omega_{\rm p}$ is the plasma frequency

$$\omega_{\rm p} = \frac{4\pi e^2}{m} n_{\rm e} \tag{A.3}$$

where m is the mass of the charge carriers (electrons, holes) and $n_{\rm e}$ their number density. γ is the reciprocal of the mean collision time of the charge carriers. Within the frame of the Drude model it is related to the d.c. electrical conductivity σ of the material by

$$\sigma = \frac{\omega_{\rm p}^2}{4\pi\gamma}. \tag{A.4}$$

The dielectric constant in the combined Drude-Lorentz model is given by

$$\epsilon(\omega) = \epsilon_0 - \sum_j \frac{\omega_{{\rm p}j}^2}{\omega^2 - \omega_{0j}^2 + i\gamma_j\omega} \tag{A.5}$$

(Bohren & Huffman 1983). The constant ϵ_0 equals unity if all existing oscillators are considered in the model. Values of ϵ_0 different from unity are required if oscillators in the far UV are not considered explicitly but are included only by their low frequency limit contribution $\omega_{\rm p}^2/\omega_0^2$ (cf. A.1). The model (A.5) automatically satisfies the Kramers-Kronig relations.

We have determined the constants ϵ_0, $\omega_{{\rm p}j}$, ω_{0j}, and γ_j from a least square fit to experimental data. Table A.1 shows the results for the fitting coefficients for the model (A.5) to experimental data for some dust materials. The fit has been performed by using the `fit` option of the GNUPLOT software. For SiC optical constants of SiC according to Laor & Draine (1993) are used. For Fe data from the CRC-handbook (Lide 1995) and from Pollak et al. (1994) have been taken.

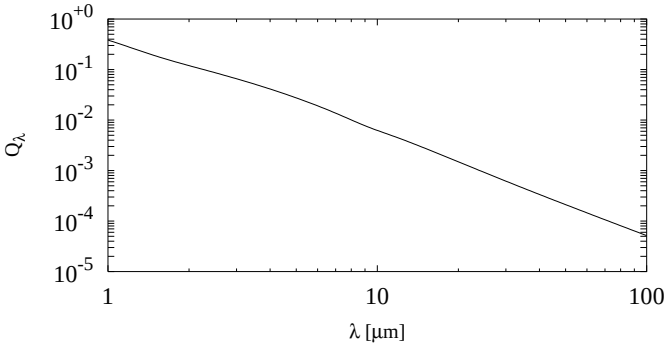

Fig. A.1. Extinction efficiency Q_λ of FeSi for 0.1 μm sized dust grains.

For FeSi we used optical reflectivity data from Degiorgi et al. (1994) and fitted a Drude-Lorentz model (A.5) using the relation between optical reflectivity and the complex dielectric coefficient (cf. Bohren & Huffman 1983). For our present calculation we use the data measured at room temperature ($T = 300\,{\rm K}$ in Degiorgi et al. 1994) since the infrared emission from dust in mass-loosing AGB stars is emitted by warm dust. This is particular important for the material FeSi, because its low-temperature optical properties are completely different from its high-temperature properties. At high temperature $T \gtrsim 200\,{\rm K}$ the material optically behaves like a metal, at lower temperature like an insulator. The strong temperature dependence of the properties of FeSi may be seen, e.g., from Fig. 3 of Ferrarotti et al. (2000). The results of our fit of the high-temperature data of the optical reflectivity to a Drude-Lorentz model are given in Table A.1. The absorption efficiency Q_λ calculated for a spherical dust grain with radius 0.1 μm is shown in Fig. A.1 as an example.

Appendix B: Thermodynamic data for Fe-Si compounds

For the molecules FeSi and NiSi the free enthalpies of formation ΔG from the free atoms are calculated using the statistical mechanics formula for $c_{\rm p}$ and S (cf. introduction to the JANAF tables, Chase et al. 1985, for instance).

The molecular data (dissocation energy, bond length, vibrational frequency) are taken from vander Auwera-Mahieu, McIntyre & Drowart (1969). The temperature dependence of ΔG is fitted by a polynomial of the form

$$\Delta G(T) = \frac{a}{T} + b + cT + dT^2 + eT^3\,, \qquad \text{(B.1)}$$

following Sharp & Huebner (1990). The coefficients $a, \ldots, e$ are given in Table A.2.

Thermodynamic data for the solid compounds of Fe, Ni, and Si are taken from Barin (1992). The free enthalpy of formation from free atoms is fitted, again, by the polynomial (B.1). Results are presented in Table A.2.

References

Anders, E., & Grevesse, N. 1989, Geochim. Cosmochim. Acta, 53, 197

Barin, I. 1992, Thermodynamical Data of Pure Substances (Verlag Chemie, Weinheim)

Beck, H. K. B., Gail, H.-P., Henkel, R., & Sedlmayr E. 1992, A&A, 265, 626

Bell, K. R., & Lin, D. N. C. 1994, ApJ, 427, 987

Bernatowicz, T. J., Cowsik, R., Gibbons, P. C., et al. 1996, ApJ, 472, 760

Bieging, J. H., & Latter, W. B. 1994, ApJ, 422, 765

Bohren, C. F., & Huffman, D. R. 1983, Absorption and Scattering of Light by Small Particles (John Wiley & Sons, New York)

Boothroyd, A. I., & Sackman, I.-J. 1999, ApJ, 510, 232

Busso, M., Gallino, R., & Wasserburg, G. J. 1999, ARA&A, 37, 239

Chase, Jr. M. W., Davies, C. A., Downey, Jr. J. R., et al. 1985, JANAF Thermodynamic Tables, National Institute of Standards and Technology, Gaithersburg

Chen, P. S., & Kwok, S. 1993, ApJ, 416, 769

Cherchneff, I. 1998, in The Molecular Astrophysics of Stars and Galaxies, ed. T. W. Hartquist, & D. A. Williams (Clarendon Press, Oxford), 265

Chigai, T., Yamamoto, T., & Kozasa, T. 1999, ApJ, 510, 999

Degiorgi, L., Hunt, M. B., Ott, H. R., et al. 1994, Europhys. Lett. 28, 341

Ebel, D. S., & Grossman, L. 2000, Geochim. Cosmochim. Acta, 64, 339

Edvardsson, B., Andersen, J., Gustafsson, B., et al. 1993, A&A, 275, 101

Fegley, B., & Lodders, K. 1994, Icarus, 110, 117

Ferrarotti, A., Gail, H.-P., Degiorgi, L., & Ott, H. R. 2000, A&A, 357, L13

Ferrarotti, A. S., & Gail, H.-P. 2001, A&A, 371, 133, Paper II

Gail, H.-P., & Sedlmayr, E. 1998a, in The Molecular Astrophysics of Stars and Galaxies, ed. T. W. Hartquist, & D. A. Williams (Clarendon Press, Oxford), 287

Gail, H.-P., & Sedlmayr, E. 1998b, Faraday Disc., 109, 303

Gail, H.-P., & Sedlmayr, E. 1999, A&A, 347, 594, Paper I

Gautschy, A., & Saio, H. 1995, ARA&A, 33, 75

Gilman, R. C. 1969, ApJ, 155, L185

Glassgold, A. E. 1996, ARA&A, 34, 241

Grevesse, N., & Noels, A. 1993, in Origin and Evolution of the Elements, ed. N. Prantzos, E. Vangioni-Flam, & M. Cassé (Cambridge University Press, Cambridge), 15

Groenewegen, M. A. T., & de Jong, T. 1998, A&A, 337, 797

Groenewegen, M. A. T., van den Hoek, L. B., & de Jong, T. 1995, A&A, 293, 381

Grossman, L. 1972, Geochim. Cosmochim. Acta, 36, 597

von Helden, G., Tielens, A. G. G. M., van Heijnsbergen, D., et al. 2000, Science, 288, 313

Iben, Jr. I. 1991, ApJS ,76, 55

de Jager, C., Nieuwenhuijzen, H., & van der Hucht, K. A. 1988, A&AS, 72, 259

Jaschek, C., & Jaschek, M. 1987, The classification of stars (Cambridge University Press, Cambridge etc.)

Jeong, K. S. 2000, Dust Shells around oxygen-rich Miras and Long-Period Variables, Thesis, Technical University, Berlin

Jorissen, A., & Knapp, G. R. 1998, A&AS, 129, 363

Jorissen, A., Frayer, D. T., Johnson, H. R., Mayor, M., & Smith, V. V. 1993, A&A, 271, 463

Jura, M. 1988, ApJS, 66, 33

Kerschbaum, F. 1999, A&A, 351, 627

Kerschbaum, F., & Hron, J. 1996, A&A, 308, 489

Kozasa, T., Dorschner, J., Henning, T., & Stognienko, R. 1996, A&A, 307, 551

Kubaschewski, O., & Alcock, C. B. 1983, Metallurgical Thermochemistry, 5th Ed. (Pergamon Press, Oxford)

Landolt-Börnstein 1968, Zahlenwerte und Funktionen, vol. 5b, ed. K. Schäfer (Springer Verlag, Heidelberg)

Laor, A., & Draine, B. T. 1993, ApJ, 402, 441

Lattanzio, J., & Forestini, M. 1999, in Asymptotic Giant Branch Stars, ed. T. Le Bertre, A. Lèbre, & C. Waelkens, IAU Symp., 191, 31

Lattimer, J. M. , Schramm, D. N., & Grossman, L. 1978, ApJ, 219, 230

Lide, R. D. 1995, CRC Handbook of Chemistry and Physics, 76th ed. (CRC Press, Boca Raton etc.)

Lloyd Evans, T. 1984, MNRS, 204, 985

Lloyd Evans, T., & Little-Marenin, I. R. 1999, MNRAS, 304, 421

Lodders, K., & Fegley, Jr. B. 1995, Meteoritics, 30, 661

Lodders, K., & Fegley, Jr. B. 1997, in Astrophysical Implications of the Laboratory Study of Presolar Material, ed. T. J. Bernatovicz, & E. K. Zinner, American Instit. of Phys., AIP Conf. Proc., 402, 391

Lodders, K., & Fegley, Jr. B. 1999, in Asymptotic Giant Stars, ed. T. Le Bertre, A. Lébre, & C. Waelkens, IAU Symp., 191, 279

Meader, A., & Meynet, G. 1988, A&AS, 76, 411

Molster, F. J. 2000, Thesis, University of Amsterdam

Nagahara, H., & Ozawa, K. 1996, Geochim. Cosmochim. Acta, 60, 1445

Pollack, J. B., Hollenbach, D., Beckwith, S., et al. 1994, ApJ, 421, 615

Råback, P. 1999, Modeling of Sublimation Growth of Silicon Carbide Crystals, Dissertation Helsinki University of Technology, ISBN 952-9821-54-9

Sahai, R., & Liechti, S. 1995, A&A, 293, 198

Saxena, S. K., & Eriksson, G. 1986, in Chemistry and Physics of Terrestrial Planets, ed. S. K. Saxena (Springer, New York etc.), 30

Scalo, J. M. 1974, ApJ, 194, 361

Scalo, J. M., & Ross, J. E. 1976, A&A, 48, 219

Schaller, G., Schaerer, D., Meynet, G., & Maeder, A. 1992, A&AS, 96, 269

Sharp, C. M., & Huebner, W. F. 1990, ApJS, 72, 417

Sharp, C. M., & Wasserburg, G. J. 1995, Geochim. Cosmochim. Acta, 59, 1633

Smith, V. V. 1997, Chpt. XI in: Wallerstein G., Rev. Mod. Phys., 69, 1042
Smith, V. V., & Lambert, D. L. 1990, ApJS, 72, 387
Snow, T. P., & Witt, A. N. 1996, ApJ, 468, L65
Stephens, J. R. 1989, in Solid state astrophysics, ed. E. Busoletti, & G. Strazulla (North Holland Publ., Amsterdam), 391
van Belle, G. T., Dyck, H. M., Thompson, R. R., Benson, J. A., & Kannappan, S. J. 1997, AJ, 114, 2150
Van Eck, S., Jorissen, A., Udry, S., Mayor, M., & Pernier, B. 1998, A&A, 329, 971
vander Auwera-Mahieu, A., Mc Intyre, N. S., & Drowart, J. 1969, Chem. Phys. Lett., 4, 198
Wallerstein, G., & Knapp, G. R. 1998, ARA&A, 36, 369
Warner, B. 1968, in Origin and Distribution of the Elements, ed. L. H. Ahrens (Pergamon Press, Oxford etc.), 205
Willson, L. A. 2000, ARA&A, 38, 573
Wood, P. R. 1990a, in From Miras to Planetary Nebulae, ed. M. O. Menessier, & A. Omont, (Gif-sur-Yvette: Éditions Frontières), 67
Wood, P. R. 1990b, in Confrontation between stellar pulsation and evolution, ed. C. Cacciari, & G. Clementini, ASP Conf. Ser., 11, 355
Xiong, D. R., Deng, L., & Cheng, Q. L. 1998, ApJ, 499, 355
Zinner, E., & Amari, S. 1999, in Waelkens Asymptotic Giant Branch Stars, ed. T. Le Bertre, & A. Lèbre, C. IAU Symp., 191, 59